the toxic change in microglia or act only on the toxic subtypes of microglia.

Future prospects of studies of postmortem PD brains

Biochemical and molecular biological studies of postmortem brains in PD have greatly contributed to our understanding of PD pathogenesis at the molecular level, though interpretation of the data must be made with caution due to the complexity of factors in the postmortem human brain.

First, establishment of brain banks including control brains are the most important to obtain an adequate number of samples. It is desired to establish the same and common system of brain banks in order to exchange brain samples among many brain banks.

Second, precise clinical records of the patients including drug administration are essential.

Third, one must consider that punched-out brain tissues, however small the sample is, contain various neurons and glial cells. Therefore, the precise brain location for punching-out tissues becomes highly critical. Various micropunching techniques have been developed, owing to the increased sensitivity of analytical systems, e.g., high-performance liquid chromatography (HPLC) with micro-bore columns (internal diameter <1–2 mm) for various neurotransmitters, and RT-PCR for the assay of mRNA contents. For example, the detection limit for catecholamines by using micro-bore HPLC is ~50 fmol (Nagatsu and Kokjima, 1988). Thus, even tissues of ~mg order can be analyzed.

Kanazawa's group for the first time performed single-cell analysis of CAG repeats in brains of two patients with dentatorubral-pallidoluysian atrophy (DRPLA) by using a newly developed excimer laser microdissection system to analyze somatic mosaicism in their brains (Hashida et al., 2001). They also provided the first quantitative measurements of the mRNA expression profile of AMPA receptor subunits in human single neurons from patients with amyotrophic lateral sclerosis (ALS) by means of quantitative RT-PCR with a laser micro-dissector (Kawahara et al., 2003).

Sawada's group has also established a method for single-cell analysis by laser capture micro-dissection for identification of cells by immunohistochemistry. Analysis of the effects of various biologically active compounds can now be carried out on a single cell or the same group of cells, which are isolated by laser capture microdissection and identified by immunohistochemical staining. Biochemical studies on postmortem human brains at the cellular level will further contribute to elucidation of the molecular pathology of PD, AD, and other neurodegenerative and neuropsychiatric diseases.

Acknowledgements

We dedicate this paper to Prof. Dr. Peter Riederer in commemorate his great contributions to basic research on PD. We have collaborated with Dr. Peter Riederer for many years on biochemical studies of postmortem human brains from the brain bank established by him at Würzburg University. We are very grateful to Dr. Riederer for his friendship and to Professors Dr. Hirotaro Narabyashi and Dr. Mitsuo Yoshida of Japan for having introduced us to the biochemical study of postmortem brains. We thank all of our collaborators: Drs. M. Mogi, K. Imamura, K. Ono, H. Suzuki, and Y. Hashizume for their participation in our recent work; and Drs. R. Iizuka, T. Kondo, Y. Mizuno, I. Kanazawa, and S. Kuno for supplying us postmortem brain samples from their brain banks in Japan.

References

Anglade P, Vyas S, Javoy-Agid F, Ilerreto MT, Michel PP, Marquez J, Pouatt-Prigent A, Ruberg M, Hirsch C, Agid Y (1997) Apotosis and autophagy in nigral neurons of patients with Parkinson's disease. Histol Histopathol 12: 25–31

Boka G, Anglade P, Wallach D, Javoy-Agid F, Agid Y, Hirsch H (1994) Immunocytochemical analysis of tumor necrosis factor and its receptor in Paekinson's disease. Neurosci Lett 172: 151–154

Braak H, Müller CM, Rüb U, Ackermann H, Bratzke H, de Vos Rai RAI, Del Tredici K (2006) Pathology associated with sporadic Parkinson's disease – where does it end? J Neural Transm Suppl 70: 89–97

Bringmann G, Brückner R, Münchbach M, Feinei D, God R, Wesemann W, Grote C, Herderich M, Diem S, Lesch K-P, Mössner R, Storch A (2000) Clonal-derived mammalian alkaloid with neurotoxic properties. "TaClo". In: Storch A, Collins MA (eds) Neurotoxic factors in Parkinson's disease and related disorders. Kluwer Academic Publishing/Plenum, New York, pp 145–149

Collins MA, Neafsey EJ (2000) β-Carboline analogues of MPP+ as environmental neurotoxins. In: Storch MA, Collins MA (eds) Neurotoxic factors in Parkinson's disease and related disorders. Kluwer Academic Publishing/Plenum, New York, pp 115–130

Ehringer H, Hornykiewicz O (1960) Verteilung von Noradrenalin und Dopamin (3-Hydroxytyramin) im Gehirn des Menschen und ihr Verhalten bei Erkrankungen des Extrapyramidaren Systems. Klin Wochenschr 38: 1236–1239

Foley P, Mizuno Y, Nagatsu T, Sano A, Youdim MBH, McGeer P, McGeer E, Riederer P (2000) The L-Dopa story – an early Japanese contribution. Parkinsonism Relat Disord 6: 1–1

Grima B, Lamouroux A, Boni C, Julien J-F, Javoy-Agid F, Mallet J (1987) A single human gene encoding multiple tyrosine hydroxylases with different predicted functional characteristics. Nature 326: 707–711

Hartmann A, Hunot S, Michel PP, Muriel MP, Vyas S, Faucheux BA, Mouatt-Prignet A, Turmel H, Srinivasan A, Ruberg M, Evans GI, Agid Y, Hirsch EC (2000) Caspase-3: a vulnerable factor and a final effector in the apoptotic cell death of dopaminergic neurons in Parkinson's disease. Proc Natl Acad Sci USA 97: 2875–2880

Hashida H, Goto J, Suzuki T, Jeong S-Y, Masuda N, Ooie T, Tachiiri Y, Tsuchiya H, Kanazawa I (2001) Single cell analysis of CAG repeat in brains of dentatorubral-pallidoluysian atrophy (DRPLA). J Neurol Sci 190: 87–93

Haycock JW (2002) Species differences in the expression of multiple tyrosine hydroxylase protein isoforms. J Neurochem 81: 974–953

Hayley S, Anisman H (2005) Multiple mechanisms of cytokine action in neurodegenerative and psychiatric states: neurochemical and molecular substrates. Curr Pharmac Design 11: 947–962

Hirsch EC, Hunot S, Faucheux BA, Agid Y, Mizuno Y, Mochizuki H, Tatton WG, Tatton N, Olanow WC (1999) Dopaminergic neurons degenerate by apoptosis in Parkinson's disease. Mov Disord 14: 383–385

Hirsch EC, Breidert T, Rousselet E, Hunot S, Hartmann A, Michel PP (2003) The role of glial reaction and inflammation in Parkinson's disease. Ann NY Acad Sci 991: 214–228

Ichikawa S, Ichinose H, Nagatsu T (1990) Multiple mRNAs of monkey tyrosine hydroxylase. Biochem Biophys Res Commun 173: 1331–1336

Ichinose H, Sumi-Ichinose C, Ohye T, Hagino Y, Fujit K, Nagatsu T (1992) Tissue-specific alternative splicing of the first exon generates two types of mRNAs in human aromatic L-amino acid decarboxylase. Biochemistry 31: 11546–11550

Ichinose H, Ohye T, Fujita K, Yoshida M, Ueda S, Nagatsu T (1993) Increased heterogeneity of tyrosine hydroxylase in humans. Biochem Biopys Res Commun 195: 158–165

Ichinose H, Ohye T, Fujita K, Pantucek F, Lange K, Riederer P, Nagatsu T (1994) Quantification of mRNA of tyrosine hydroxylase and aromatic L-amino acid decarboxylase in the substantia nigra in Parkinson's disease and schizophrenia. J Neural Transm [P-D Sect] 8: 149–158

Imamura K, Hishikawa N, Sawada M, Nagatsu T, Yoshida M, Hashizume Y (2003) Distribution of major histocompatibility complex class II-positive microglia and cytokine profile of Parkinson's disease brain. Acta Neuropatholgica 106: 518–526

Imamura K, Hishikawa N, Ono K, Suzuki H, Sawada M, Nagatsu T, Yoshida M, Hashizume Y (2005) Cytokine production of activated microglia and decrease in neurotrophic factors of neurons in the hippocampus of Lewy body disease brains. Acta Neuropathol 109: 141–150

Jellinger KA (2005) Cell death mechanism in Parkinson's disease. J Neural Transm 107: 1–29

Kaneda N, Kobayashi K, Ichinose H, Kishi F, Nakazawa A, Kurosawa Y, Fujita K, Nagatsu T (1987) Isolation of a novel cDNA clone for human tyrosine hydroxylase: alternative RNA splicing produces four kinds of mRNA from a single gene. Biochem Biophys Res Commun 146: 971–975

Kawahara Y, Kwak S, Sun H, Ito K, Hashida H, Aizawa H, Jeong S-Y, Kanazawa I (2003) Human spinal motoneurons express low relative abundance of GluR2 mRNA: an implication for exicitotoxicity in ALS. J Neurochem 85: 680–689

Kobayashi K, Kaneda N, Ichinose H, Kishi F, Nakazawa A, Kurosawa Y, Fujita K, Nagatsu T (1988) Structure of the human tyrosine hydroxylase gene: alternative splicing from a single gene accounts for generation of four mRNA types. J Biochem 103: 907–912

Kotake Y, Tasaki Y, Makino S, Ohta S, Hirobe M (1995) 1-Benzyl-1,2,3,4-tetrahydroisoquinoline as a parkinsonism-inducing agent: a novel endogenous amine in mouse brain and parkinsonian CSF. J Neurochem 65: 2633–2638

Langston JW, Ballard P, Tetrud JW, Irwin I (1983) Chronic parkinsonism in humans due to a product of meperidine-analog synthesis. Science 219: 979–980

Langston JW, Forno JS, Tetrud J, Reeves AG, Kaplan JA, Karluk D (1999) Evidence of active nerve cell degeneration in the substantia nigra of humans years after 1-methyl-4-phenyl-1,2,3,6-tetrahydropyridine exposure. Ann Neurol 46: 598–605

Lloyd K, Hornykiewicz O (1970) Parkinson's disease: activity of L-DOPA decarboxylase in discrete brain regions. Science 171: 1075–1078

Lloyd KG, Davidson L, Hornykiewicz O (1975) The neurochemistry of Parkinson's disease: effect of L-dopa therapy. J Pharmacol Exp Ther 195: 453–464

Matsubara K (2000) N-Methyl-β-carbolinium neurotoxins in Parkinson's disease. In: Storch A, Collins MA (eds) Neurotoxic factors in Parkinson's disease and related disorders. Kluwer Academic Publishing/ Plenum, New York, pp 131–143

McGeer PL, McGeer EG (1976) Enzymes associated with the metabolism of catecholamine, acetylcholine and GABA in human controls and patients with Parkinson's disease and Huntington's chorea. J Neurochem 26: 65–76

McGeer PL, Itagaki S, Boyes BE, McGeer EG (1988) Reactive microglia are positive for HLA-DR in the substantia nigra of Parkinson's disease and Alzheimer's disease brains. Neurology 38: 1285–1291

McGeer PL, McGeer EG (1995) The inflammatory response system of brain, implications for therapy of Alzheimer's and other neurodegenetative diseases. Brain Res Rev 21: 195–218

McGeer PL, Schwab C, Parent A, Doudet D (2003) Presence of reactive microglia in monkey substantia nigra years after 1-methyl-4-phenyl-1,2,3,6-tetrahydropyridine administration. Ann Neurol 54: 599–604

Mizuno Y, Hattori N, Yoshino H, Hatano Y, Satoh K, Tomiyama H, Li Y (2006) Progress in familial Parkinson's disease. J Neural Transm Suppl 70: 191–204

Mogi M, Harada M, Kiuchi K, Kojima K, Kondo T, Narabayashi H, Rausch D, Riederer P, Jellinger K, Nagatsu T (1988a) Homospecific activity (activity per enzyme protein) of tyrosine hydroxylase increases in Parkinsonian brain. J Neural Transm 72: 77–81

Mogi M, Harada M, Kojima K, Inagaki H, Kondo T, Narabayashi H, Arai T, Teradaira R, Fujita K, Kiuchi K, Nagatsu T (1988b) Sandwich enzyme immunoassay of dopamine-β-hydroxylase in cerebrospinal fluid from control and Parkinsonian patients. Neurochem Int 12: 187–191

Mogi M, Harada M, Riederer P, Narabayashi H, Fuita K, Nagatsu T (1994) Tumor necrosis factor-α (TNF-α) increases both in the brain and in the cerebrospinal fluid from parkinsonian patients. Neurosci Lett 165: 208–210

Mogi M, Togari A, Ogawa M, Ikeguchi K, Shizuma N, Fan D-S, Nakano I, Nagatsu T (1998) Effects of repeated systemic administration of 1-methyl-4-phenyl-1,2,3,6-tetrahydripyridine (MPTP) to mice on interleukin-1β and nerve growth factor in the striatum. Neurosci Lett 250: 25–28

Mogi M, Togari A, Tanaka K, Ogawa N, Ichinose H, Nagatsu T (1999) Increase in level of tumor necrosis factor (TNF)-α in 6-hydroxydopamine-lesioned striatum in rats is suppressed by immunosupressant FK506. Neurosci Lett 289: 165–168

Mogi M, Nagatsu T (1999) Neurotrophins and cytokines in Parkinson's disease. Adv Neurol 80: 135–139

Mogi M, Togari A, Kondo T, Mizuno Y, Komure O, Kuno S, Ichinose H, Nagatsuu T (2000) Caspase activities and tumor necrosis-α R1 (p55) level were elevated in the subsantia nigra from Parkinsonian brain. J Neural Transm 107: 335–341

Nagatsu T, Kato T, Numata (Sudo) Y, Ikuta K, Sano M, Nagatsu I, Kondo Y, Inagaki S, Iizuka R, Hori A, Narabayashi H (1977) Phenylethanolamine N-methyltransferase and other enzymes of catecholamine metabolism in human brain. Clin Chim Acta 75: 221–232

Nagatsu T, Yamaguchi T, Kato T, Sugimoto T, Matsuura S, Akino M, Nagatsu I, Iizuka R, Narabayashi H (1981) Biopterin in human brain and urine from controls and parkinsonian patients: application of a new radioimmunoassay. Clin Chim Acta 109: 305–311

Nagatsu T, Yamaguchi T, Rahman MK, Trocewicz J, Oka K, Hirata Y, Nagatsu I, Narabayashi H, Kondo T, Iizuka R (1984) Catecholamine related-enzymes and the biopterin cofactor in Parkinson's disease. Adv Neurol 40: 467–473

Nagatsu T, Horikoshi T, Sawada M, Nagatsu I, Kondo T, Iizuka R, Narabayashi H (1986) Biosynthesis of tetrahydrobiopterin in parkinsonian human brain. Adv Neurol 45: 223–226

Nagatsu T, Kojima K (1988) Application of electrochemical detection in high-performance liquid chromatography to the assay of biologically active compounds. Trend Anal Chem 7: 21–27

Nagatau T (1990) Changes in tyrosine hydroxylase in parkinsonian brains and in the brain of MPTP-treated mice. Adv Neurol 53: 207–214

Nagatsu T (1997) Isoquinoline neurotoxins in the brain and Parkinson's disease. Neurosci Res 29: 99–111

Nagatsu T, Mogi M, Ichinose H, Togari A, Riederer P (1999) Cytokines in Parkinson's disease. Neurosci News 2: 88–90

Nagatsu T, Mogi M, Ichinose H, Togari F (2000a) Cytokines in Parkinson's disease. J Neural Transm Suppl 58: 143–151

Nagatsu T, Mogi M, Ichinose H, Togari F (2000b) Changes in cytokines and neurotrophins in Parkinson's disease. J Neural Transm 60: 277–290 Suppl 60: 277–290

Nagatsu T (2002a) Amine-related neurotoxins in Parkinson's disease: past, present, and future. Neurotoxicol Teratol 24: 565–569

Nagatsu T (2002b) Parkinson's disease: changes in apoptosis-related factors suggesting possible gene therapy. J Neural Transm 109: 731–745

Nagatsu T, Sawada M (2005) Inflammatory process in Parkinson's disease: role for cytokines. Curr Pharmaceut Design 11: 999–1016

Nagatsu T, Sawada M (2006) Cellular and molecular mechanisms of Parkinson's disease: neurotoxins, causative genes, and inflammatory cytokines. Cell Mol Neurobiol 26: 779–800

Naoi M, Maruyama W, Dostert P, Hashizume Y, Nakahara D, Takahashi T, Ota M (1996) Dopamine-derived endogenous 1(R), 2(N)-dimethyl-6,7-dihydroxy-1,2,3,4-tetrahydroisoquinoline, N-methyl-(R)-salsolinol, induced parkinsonism in rats: biochemical, pathological and behavioral studies. Brain Res 709: 285–295

Ohye T, Ichinose H, Ogawa M, Yoshida M, Nagatsu T (1995) Alterations in multiple tyrosine hydroxylase mRNAs in the substantia nigra, locus coeruleus and adrenal gland of MPTP-treated Parkinsonian monkeys. Neurodegeneation 4: 81–85

Rausch W-D, Hirata Y, Nagatsu T, Riederer P, Jellinger K (1988) Tyrosine hydroxylase activity in caudate nucleus from Parkinson's disease: effects of iron and phosphorylating agents. J Neurochem 50: 202–208

Riederer P, Rausch W-D, Birkmayer W, Jellinger K, Seemann D (1978) CNS modulation of adrenal tyrosine hydroxylase in Parkinson's disease and metabolic encepahlopathies. J Neural Transm Suppl 14: 121–131

Riederer P, Reichmann H, Janetzky B, Sian J, Lesch K-P, Lange KW, Double KL, Nagatsu T, Gerlach M (2001) Neural degeneration in Parkinson's disease. In: Calne D, Calne S (eds) Parkinson's disease: Adv Neurol 86. Lippincott Williams & Wilkins, Philadelphia, pp 125–136

Rogers J, Kovelowski CJ (2003) Inflammatory mechanisms in Parkinson's disease. In: Wood PL (ed) Neuroinflammation. Humana Press, Totowa, New Jersey, pp 391–403

Sano I (1960) Biochemistry of the extrapyramidal system. Shinkei Kenyu No Shinnpo (Adv Neurol Sci) 5: 42–48; Translated into English (by Sano A) (2000) Parkinsonism Relat Disord 6: 303–306

Sawada M, Nagatsu T, Nagatsu I, Ito K, Iizuka R, Kondo T, Narabayashi H (1985) Tryptophan hydroxylase activity in the brains of controls and parkinsonian patients. J Neural Transm 62: 107–115

Sawada M, Hirata Y, Arai H, Iizuka R, Nagatsu T (1987) Tyrosine hydroxylase, tryptophan hydroxylase, biopterin, and neopterin in the brains of normal controls and patients with senile dementia of Alzheimer type. J Neurochem 48: 760–764

Sawada M, Imamura K, Nagatsu T (2006) Role of cytokines in inflammatory process in Parkinson's disease. J Neural Transm Suppl 70: 373–381

Trocewicz J, Oka K, Nagatsu T, Nagatsu I, Iizuka R, Narabayashi H (1982) Phenylethanolamine N-methyltransferase activity in human brains. Biochem Med 27: 317–324

Vilhardt F, Plastre O, Sawada M, Suzuki K, Wiznerowicz M, Kiyokawa E, Trono D, Krause K-H (2002) The HIV-1 Nef protein and phagocyte NADPH oxidase activation. J Biol Chem 277: 42136–42143

Pflugers Arch - Eur J Physiol (2008) 455:829–838
DOI 10.1007/s00424-007-0339-7

Early and late activation of the voltage-gated proton channel during lactic acidosis through pH-dependent and -independent mechanisms

Hirokazu Morihata · Junko Kawawaki · Masako Okina · Hiromu Sakai · Takuya Notomi · Makoto Sawada · Miyuki Kuno

Received: 10 June 2007 / Accepted: 27 August 2007 / Published online: 18 September 2007

Abstract Voltage-gated proton (H^+) channels play a pivotal role in compensating charge and pH imbalances during respiratory bursts in phagocytes. Lactic acidosis is a clinically important metabolic condition accompanying various tissue disorders in which the extracellular pH and the intracellular pH often change in parallel. In this study, we investigated the responses of the H^+ channel in microglia to lactate-induced pH disturbances using the perforated-patch recordings. Na-lactate (pH 6.8) acidified the cells and activated the H^+ channel within 5 min. This early activation was correlated with increases in the pH gradient across the plasma membrane (ΔpH) and was dose-dependent over a concentration range of 10–150 mM. At 10 mM, the change in ΔpH was only slight, but the H^+ currents continued to increase over an hour after the cell acidosis was stabilized. Prolonged exposure to lactate (10–20 mM, >1 h) increased the amplitude by two to threefold. The late activation was not explained by increased ΔpH but by changes in the property of the channel per se. Pretreatment with staurosporine and chelerythrine, inhibitors for protein kinase C, prevented the late activation. These results suggest that the H^+ channel could be activated greatly during long-lasting lactic acidosis through both ΔpH-dependent and -independent mechanisms.

Keywords Proton current · Lactic acid · Acidosis · Protein kinase C · pH

H. Morihata · M. Okina · H. Sakai · T. Notomi · M. Kuno (✉)
Department of Physiology,
Osaka City University Graduate School of Medicine,
Abeno-ku, Osaka 545-8585, Japan
e-mail: kunomyk@med.osaka-cu.ac.jp

J. Kawawaki
Central Laboratory,
Osaka City University Graduate School of Medicine,
Osaka 545-8585, Japan

M. Sawada
Department of Brain Life Science,
Research Institute of Environmental Medicine,
Nagoya University,
Nagoya 464-8601, Japan

M. Kuno
Department of Molecular Physiology, Division of Intracellular Metabolism, National Institutes of Natural Sciences,
Okazaki 444-8585, Japan

Introduction

Voltage-gated proton (H^+) channels, first described in snail neurons [33], are characterized by extremely high selectivity for H^+ and large H^+ effluxes [1]. They play a pivotal role in the respiratory bursts during phagocytosis [5, 12, 23]. It is deduced, from the electrophysiological properties, that the H^+ channels respond to changes in both extracellular pH (pH_o) and intracellular pH (pH_i). The activation thresholds and the driving forces for H^+ efflux through the channel are determined primarily by the pH gradient across the plasma membrane ($\Delta pH = pH_o - pH_i$). Thus, the effects of pH_i and pH_o on the voltage dependence are reciprocal: H^+ channels are activated at more positive voltages by decreases in pH_o, but at more negative voltages by decreases in pH_i. Pathological conditions, such as hypoxia, ischemia, injury and degenerating diseases, are accompanied by a disturbance of the pH homeostasis: pH_i and pH_o often change in parallel and interfere mutually. Therefore, tissue acidosis may increase or decrease ΔpH. Lactic acidosis is a clinically important metabolic acidosis and fits this case [10, 22, 29, 32].

The lactic acid generated by anaerobic glycolysis may accumulate in tissue. Lactate-induced extracellular acidification stimulates H^+-sensing channels such as the acid-sensing Na^+ channels (ASIC) [14]. The behavior of H^+ channels might, however, be more complicated. If pH_i is decreased more than pH_o, the channel would be activated. In contrast, the channel must be inhibited when the drop of pH_i is smaller than that of pH_o. Our previous study showed that a high concentration (150 mM) of lactate increased ΔpH [22], but the concentration was too high to generalize the results to the case of moderate lactic acidosis. Therefore, the dose-dependent effect of lactate on the ΔpH should be evaluated. In addition, lactic acid induces a variety of cellular responses, for instance, mitochondrial dysfunction, cell swelling, and production of free radicals, leading to deleterious effects on cellular functions [2, 10, 17, 22, 25, 32]. Besides the direct effects of ΔpH, the subsequent biological actions could affect the channel activity. To resolve these issues, it is essential to measure the H^+ channel currents from the cells exposed to lactic acidosis. However, the lactate-mediated cell acidosis could not be introduced under the whole-cell clamp configuration in which pH_i is controlled by the pipette solution. In addition, modulation of the H^+ channel activity through second messenger pathways, such as activation by protein kinase C [4], was often hampered by the intracellular dialysis.

This study focused on investigating the dose- and time-dependent behavior of the H^+ channel under lactic acidosis using the perforated-patch recordings in microglia which expresses the H^+ channel consistently [6, 7, 21, 22]. The perforated-patch recordings appear to be most suitable for minimizing perturbation of the intracellular environment and preserving cellular buffer actions. Electrophysiological analyses permitted the estimation of cell acidosis and ΔpH-dependent events. The data suggested that the H^+ channel would be activated during lactic acidosis through ΔpH-dependent and -independent mechanisms.

Materials and methods

Cells A rat microglial cell line (GMI-R1) [28] was cultured in the Eagle's MEM containing 1 ng/ml recombinant mouse GM-CSF (Peprotec), 10 ng/ml insulin, 10 mM glucose, 100 U/ml penicillin, 0.1 mg/ml streptomycin, 0.25 ng/ml amphotericin B, and 10% fetal calf serum. Cells were plated at a density of $1.0–2.0\times10^5$ cells/ml on coverslips and were incubated at 37°C in a 95% air–5% CO_2 atmosphere. The culture medium was changed every 3–4 days. GMI-R1 cells preserve microglial characteristics [28] and exhibit H^+ channels consistently [21]. The properties of the H^+ channels share the same characteristics with those in microglia in primary culture [6, 7, 21, 22].

Solutions The standard Ringer solution contained (in millimolar): 145 NaCl, 5 KCl, 1 $CaCl_2$, 1 $MgCl_2$, and 10 HEPES (pH 7.3). The Na^+-free K^+-rich solution and the $NMDG^+$ solution were made by replacing NaCl with either KCl or *N*-methyl-D-glucamine (NMDG) chloride. To load cells with NH_4^+, NaCl was replaced by 40 mM NH_4Cl. Na-lactate solutions were made with 10–150 mM Na-lactate, 0 or 5 mM KCl, 1 mM $CaCl_2$, 1 mM $MgCl_2$, 10 mM Hepes (pH 6.8). The osmolarities were adjusted by adding either Na-isethionate or NaCl. There was no consistent difference in the results between the solutions containing Na-isethionate and NaCl. All solutions were supplemented with 10 mM glucose and 0.1% bovine serum albumin (BSA). The osmolarities of the solutions were measured using a freezing-point depression osmometer (OS osmometer, Fiske, MA, USA) and were maintained between 285 and 300 mosmol/l.

Electrophysiological recordings In perforated-patch recordings, the standard pipette solutions contained: 150 mM Cs-methansulfonate, 3 mM $MgCl_2$, 1 mM EGTA, 10 mM Hepes, and amphotericin B (500 μg/ml; pH 7.3). The standard extracellular solution was 150 mM Na-isethionate, 1 mM $CaCl_2$, 1 mM $MgCl_2$, 10 mM Hepes, 10 mM glucose, and 0.1% BSA (pH 7.3). As the microglia express K^+ channels, K^+ was generally omitted from both intracellular and extracellular solutions. The K^+ concentration (0–5 mM) did not affect the results in voltage-clamped cells in which the holding potential was maintained. In most of recordings, 50 μM 4,4′-diisothiocyano-2,2′-stilbenedisulfonic acid (DIDS), a Cl^- channel blocker, was added to the bath solution. The buffer molecules (Hepes) could not pass through the amphotericin B pores [20], and so the pH_i was controlled by the intrinsic pH buffers. The membrane potential was measured under the current-clamp configuration in the standard Ringer solution: Cs-methanesulfonate in the pipette solution was replaced by K-gluconate. To characterize the electrophysiological properties of the channel per se, H^+ currents were recorded in whole-cell recordings. Major ions (Na^+, K^+ and Cl^-) were removed from both bath and pipette solutions. The pipette contained 65 mM NMDG-aspartate, 3 mM $MgCl_2$, 1 mM BAPTA, 120 mM Mes (pH 5.5–6.5). The pH was adjusted by CsOH or KOH. The bath contained (in millimolar): 75 NMDG-aspartate, 100 Hepes, 1 $MgCl_2$, 1 $CaCl_2$ and 50 μM DIDS (pH 7.3). Ten millimolar glucose and 0.1% BSA were added into the bath solutions. The osmolarities of the solutions were maintained between 280 and 290 mosmol/l.

The reference electrode was a Ag–AgCl wire connected to the bath solution through a Ringer-agar bridge. The liquid junction potential was corrected before formation of the gigaseal in all experiments. The pipette resistances ranged between 5 and 15 MΩ. Current or voltage signals

were recorded with an amplifier (Axopatch 200A, Axon Instruments, Foster City, CA, USA), digitized at 2 kHz with an analog-digital converter (Digidata 1200, Axon Instruments), and analyzed using pCLAMP software (Axon Instruments). Proton currents were evoked by depolarization pulses (1–4 s) applied at the holding potentials (−80–0 mV) every 10–20 s. Leak currents were estimated from the linear portion of the current-voltage (*I–V*) relation at voltages lower than the threshold potential for the H^+ channel. The leak currents were subtracted from the current records. All experiments were carried out at room temperature (22–24°C) [18].

Data analysis The activation process was fitted with a single exponential function after a delay time, giving estimates of the steady-state currents and the activation time constants (τ_{act}). The reversal potentials (V_{rev}) were obtained by either the tail-current method or the repolarization-pulse method [11, 18, 20]. In the former, the *I–V* relationships were obtained from instantaneous tail currents at different voltages following a constant voltage pulse (+100 mV, 1–2 s). In the latter, the *I–V* relationships were obtained by applying 20-ms-long repolarization voltage-ramps at the end of 2-s-long depolarization (40–100 mV). Subtraction of the leak and capacitive currents after a short (20 ms) depolarization yielded the net *I–V* curves for the H^+ currents. The V_{rev}s were obtained from the zero-current voltages. In the perforated-patch recordings, the tail current method was used, as the higher access resistance might generate voltage error during the short repolarization voltage-ramp. Data are means±SEM. The statistical significances ($p<0.05$) were evaluated using Student's unpaired *t* test, unless described otherwise.

We used the cell diameter ratios to monitor cell swelling, as the increases in the cell diameters were almost proportional to the estimates using the dye-dilution method or the measurements of the cell thicknesses during swelling [22].

Measurements of intracellular pH (pH_i) The intracellular pHs (pH_i) of single cells were determined with a digital fluorescence microscopy (Attoflour, Zeiss) using a pH-sensitive fluorescent dye, 2′,7′-bis-(2-carboxyethyl)-5 (and -6) carboxyfluorescein (BCECF). Cells were plated on glass coverslips for 10–24 h and loaded with the acetoxymethyl ester form of BCECF (BCECF-AM; 1 μM) for 30 min at 37°C. After washout of the dye, the ratios of the fluorescence images (the emission wavelength ≥520 nm) excited at two wavelengths (488 and 460 nm) were measured every 10 s with 30- to 100-ms exposures. Data (80–120 pixels for each cell) for each illumination were averaged and plotted against time. Calibration of pH_i was carried out by dissipating ΔpH with 10 μM nigericin in a K^+-rich solution with known pH values [9].

TUNEL staining Apoptotic effects of PKC inhibitors were examined with the method of TdT-mediated dUTP-biotin nick end labeling (TUNEL). Briefly, cells were fixed in 4% paraformaldehyde, permeabilized in 0.1% TritonX-100/0.1% sodium citrate, and stained with fluorescein-labeled TUNEL reaction mixture (Roche). Analysis by fluorescence microscopy revealed that TUNEL-positive cells were none at 2-h treatment with 100 nM staurosporine and 2–3% at 6 h.

Substances MES, BAPTA, and BCECF-AM were purchased from Dojindo Laboratories (Kumamoto, Japan), and all other chemicals were obtained from Sigma Chemical Co. (St. Louis, MO, USA). Concentrated stock solutions of DIDS, staurosporine, and chelerythrine chloride were prepared in DMSO and that of nigericin in ethanol. The final concentrations of DMSO and ethanol were less than 0.1 and 1%, respectively, which affected neither the currents nor the cell shapes.

Results

Activation of the voltage-gated proton channel in response to cell acidosis

The whole-cell H^+ currents in microglia were characterized as slowly activating outward currents evoked by depolarization (Fig. 1a) [7, 21, 22]. As the cell inside was dialyzed continuously with the pipette solution, pH_i was determined

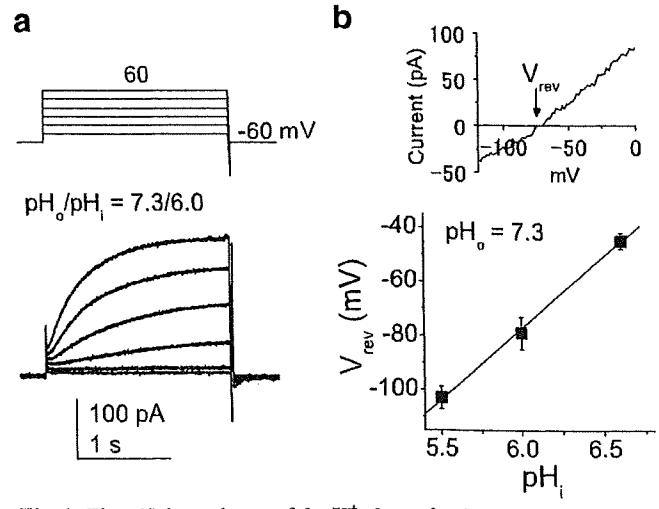

Fig. 1 The pH dependence of the H^+ channel. **a** Representative whole cell H^+ currents evoked by depolarization pulses applied at −60 mV. pH_o/pH_i=7.3/6.0. Leak currents were not subtracted. In later figures, the leak currents were subtracted from the current records. **b** The V_{rev} was obtained from the zero-current voltages of the net I–V curve (*arrow* in inset). V_{rev}s were plotted against pH_i of 5.5 (n=21), 6.0 (n=4), and 6.5 (n=5) at a constant pH_o (7.3). The relationship was linear with a slope of 53 mV/unit pH_o. Data are means±SEM

by the pH of the pipette solutions. The reversal potentials (V_{rev}) were obtained from the net I–V relation using the repolarization-pulse method (Fig. 1b, inset; see "Materials and methods"). The V_{rev} was determined by the pH gradient across the plasma membrane ($\Delta pH=pH_o-pH_i$), as the H^+ channel is highly selective for H^+. At a constant pH_o (7.3), V_{rev} was correlated with pH_i (Fig. 1b). The whole-cell clamp configuration stabilizes the pH_o and pH_i with high concentrations of pH buffers, which does not permit changes in the pH environment in response to various cellular conditions. In the perforated-patch recordings, pH_i could not be set with the pH buffers (Hepes or Mes) in the pipette solution, as the buffers did not pass through amphotericin B pores. Changes in pH_i and the channel activity could be investigated under the action of cellular buffers. However, the pH of the pipette solution (pH_p) was maintained to be constant (7.3) throughout the experiments, which might affect in pH_i. To confirm whether intracellular acidosis could be induced under this recording condition, first, we examined the behavior of the H^+ channel in response to purely intracellular acidification at constant pH_o.

Figure 2a shows averaged change of pH_i, monitored by a pH-sensitive fluorescent dye (BCECF), in cells exposed to 40 mM NH_4Cl. The pH_o was set to 7.3 throughout the experiment. The resting pH_i of single microglia was 7.32± 0.02 (n=70) in the standard Ringer solution. The pH_i was elevated transiently by application of NH_4Cl. Washout of NH_4Cl decreased pH_i rapidly, but the intracellular acidification was recovered in the Na^+-free, K^+-rich solution, which depolarized microglia (−5±5 mV, n=5). In cells incubated with 40 mM NH_4Cl for 30 min, the pH_i was 7.27±0.03 (n=52). Washout of NH_4Cl with the K^+-rich solution decreased pH_i by ~1.0 U (Fig. 2b, upper closed circle) and then returned the pH_i towards the pre-wash level. Perforated-patch recordings revealed that the H^+ channel was activated during this acutely induced cell acidosis

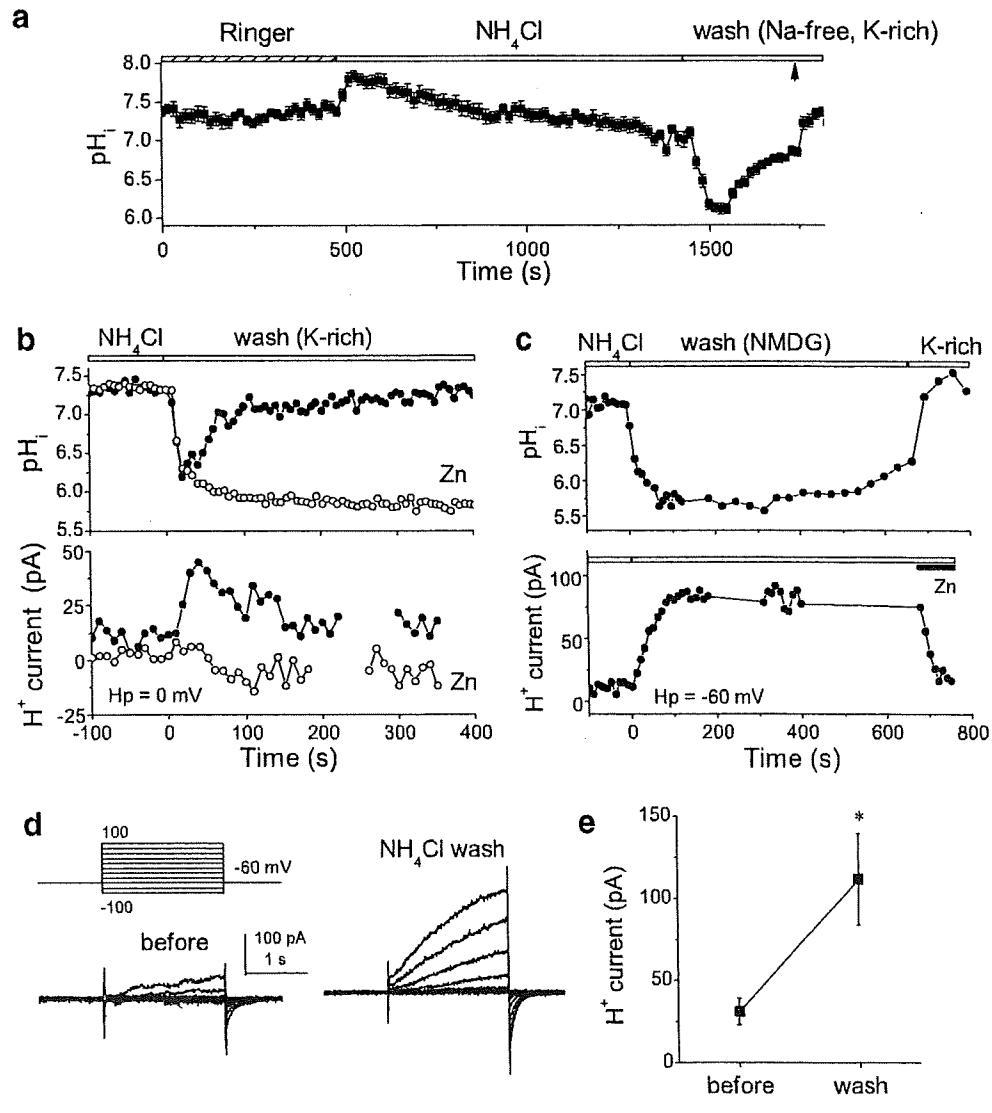

Fig. 2 Acute cell acidosis and H^+ channel activation induced by washout of pre-loaded NH_4Cl. **a** An averaged time course of changes in pH_i measured with BCECF from 15 cells exposed to 40 mM NH_4Cl. The cells were washed with a Na^+-free K^+-rich solution which depolarized the cell. Finally, nigericin was added (*arrowhead*) for calibration. pH_o was 7.3. **b** The pH_i recovery in a single cell exposed to 40 mM NH_4Cl for 30 min (*upper*). *Open symbols* represent data in the presence of 100 μM $ZnCl_2$. The H^+ current amplitudes (*lower*) were the responses evoked by a 1-s-long depolarization (−100 mV) pulse every 10 s applied at a holding potential of 0 mV. **c** pH_i responses (*upper*) and H^+ channel activation (*lower*) in hyperpolarized microglia. *Upper* NH_4Cl was replaced by a $NMDG^+$-rich solution. *Lower* The holding potential was kept at −60 mV. **d** H^+ currents evoked by step pulses applied at −60 mV in a perforated-patch before and at 3 min after washout of 40 mM NH_4Cl. **e** Mean H^+ current amplitudes measured at the end of depolarization pulse (100 mV, 2 s) before and after washout of NH_4Cl (n=9). Data are means± SEM. *p<0.05 (paired t test)

(Fig. 2b, lower closed circle). The membrane potential was held to 0 mV, except for a test pulse (100 mV, 1 s) applied every 10 s. The time course of the change in the H^+ current was similar to that in pH_i: the H^+ currents increased with the drop in pH_i and then declined along with the recovery of pH_i. The time constant of the pH_i recovery was 128±8 s (n=25), not significantly different from that for the decrease in the H^+ currents (112±13 s, n=5). Zinc, a blocker for the H^+ channel, inhibited both the pH_i recovery and the current activation (Fig. 2b, open circles), indicating that the H^+ channel contributed to the quick relief of cell acidosis in depolarized cells.

When cells were hyperpolarized by the $NMDG^+$ solution (−75±12 mV, n=3), the cell acidosis following washout of NH_4Cl was maintained until the cells were depolarized by the K^+-rich solution (Fig. 2c, upper). The H^+ channel continued to be activated in cells maintained at a holding potential of −60 mV (lower). Thus, changes in pH_i and H^+ channel activation were highly correlated: activation of the H^+ channel started by a drop in pH_i, lasted as far as the cell acidosis was maintained and terminated with the relief of the cell acidosis. Washout of NH_4Cl increased the amplitudes of the H^+ currents recorded in the perforated-patch configuration at all potentials tested (Fig. 2d), by two to fivefold (Fig. 2e). These observations showed that the present recording condition was suitable for investigating the H^+ channel activity under cell acidosis.

Lactate induces intracellular acidification and activation of the H^+ channel

We next investigated the response of the H^+ channel to lactic acidosis at a pH_o set at 6.8. The Na-lactate solutions generated sustained cell acidosis in microglia (Fig. 3a) [22]. The pH_i fell within 2–3 min to ~6.7 for 10 mM lactate, ~6.5 for 20 mM lactate and ~6.0 for 150 mM lactate. Thus, both pH_o and pH_i decreased during lactic acidosis. The subtraction gave changes in ΔpH (Fig. 3b). Lactate increased ΔpH (at 5 min) dose-dependently over 10–150 mM (Fig. 3c). The pH_i and ΔpH recovered rapidly after depolarizing the cells with the K^+-rich solution (pH 7.3; Fig. 3a and b).

The H^+ currents were increased within a few minutes after application of Na-lactate (Fig. 4a). At higher lactate concentrations, the activation was faster and more marked. Lactate increased the amplitude of the current and also facilitated the activation process upon depolarization at all potential tested (Fig. 4b); these effects were similar to the responses produced by washout of NH_4Cl. The data were fitted with a single exponential function, giving estimates of the steady-state currents and τ_{act}. The increases in the amplitudes of the steady-state currents and the decreases in τ_{act} produced by 5-min exposure of Na-lactate were dose-dependent (Fig. 4c). Lactate (150 mM) increased the current amplitudes by three to fourfold of the control and decreased the τ_{act} to one third.

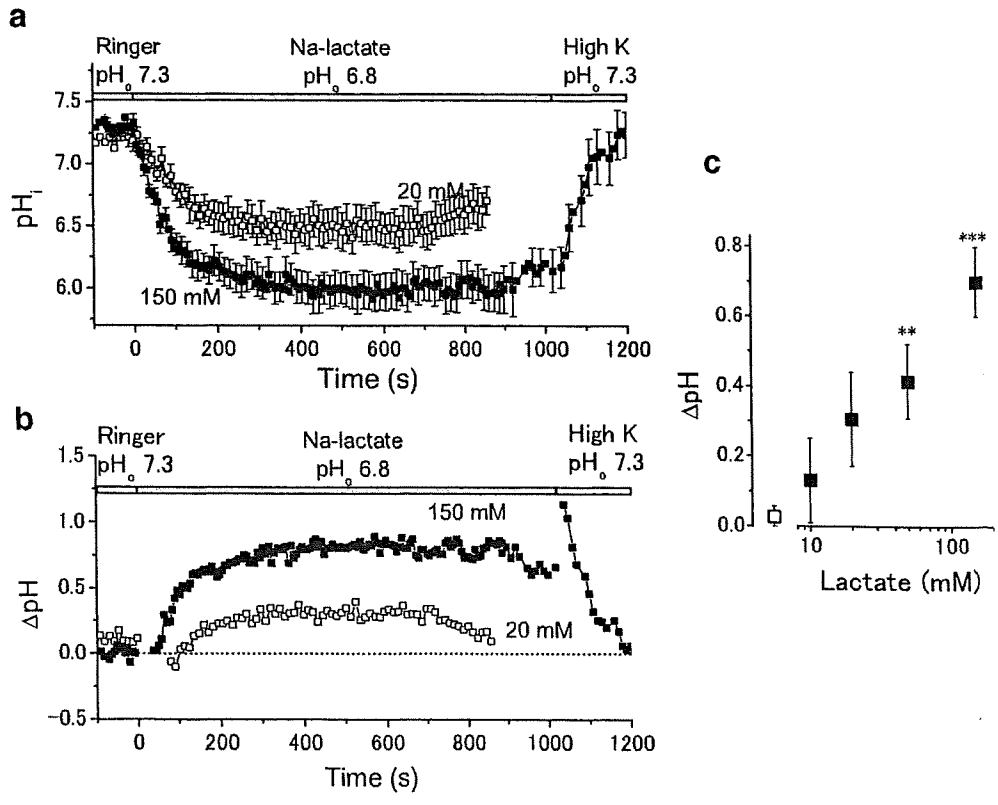

Fig. 3 pH Responses during lactic acidosis. **a** Time courses of the pH_i changes in the presence of 20 mM (*open squares*, n=8) and 150 mM Na-lactate (*closed squares*, n=7). pH_o of lactate solutions was 6.8. Washout by the Na^+-free K^+-rich solution increased pH_i quickly. **b** Time courses of the changes in ΔpH (pH_o−pH_i) for the data in **a**. **c** The dose-response relationship for ΔpH at the steady-state (5–10 min). Data are 0.03±0.03 pH unit (n=52) for control, 0.13±0.12 (n=17) for 10 mM, 0.31±0.13 (n=8) for 20 mM, 0.42±0.11 (n=8) for 50 mM, and 0.70±0.10 (n=15) for 150 mM. Data are means± SEM. **p<0.005. ***p<0.0005

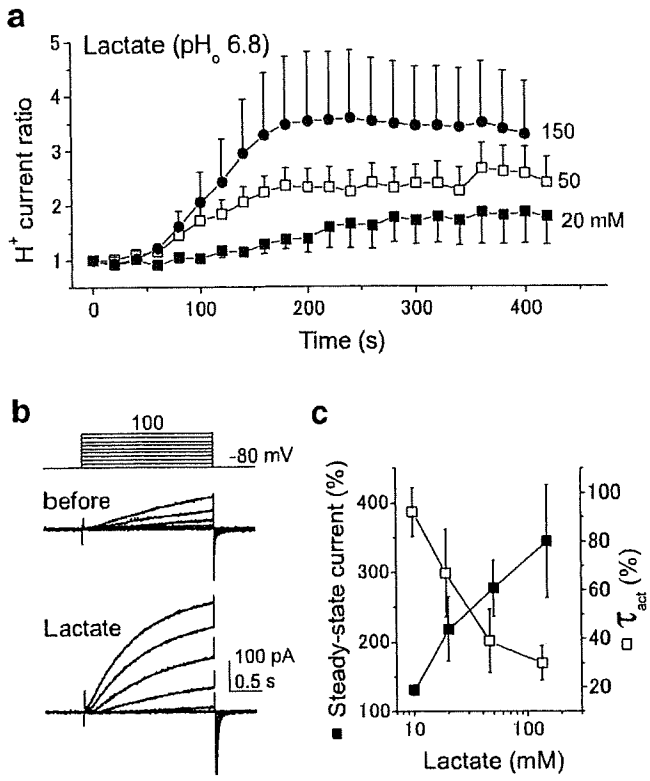

Fig. 4 H^+ channel activation during lactic acidosis. **a** Lactate-induced activation of H^+ currents under perforated-patch recordings: 20 mM (n=4–5), 50 mM (n=3–6) and 150 mM lactate (n=5). The membrane potential was −80 mV, and the H^+ current was evoked by 1-s-long depolarization (−100 mV) pulse every 20 s. The current ratio was obtained from the relative current magnitudes to those before each exposure to lactate. **b** H^+ currents before and 5 min after exposure to 50 mM Na-lactate. **c** The steady-state current amplitudes (*closed squares*) and the activation time constants (τ_{act}; *open squares*) at 5-min exposure to 10–150 mM Na-lactate. Data (mean±SEM) were obtained from the currents evoked by 80–100 mV depolarizations and expressed as percent of the control. Steady-state currents: 130±10% (n=8) for 10 mM, 220±50% (n=7) for 20 mM, 280±40% (n=6) for 50 mM, and 340±80% (n=15) for 150 mM. τ_{act}: 92±10% (n=6) for 10 mM, 67±18% (n=3) for 20 mM, 39±13% (n=3) for 50 mM and 30±7% (n=7) for 150 mM. Data are means±SEM

The *I–V* relationships of cells during the acidosis induced by washing of NH_4Cl (Fig. 5a, left) or by a 5-min exposure to 50 mM lactate (Fig. 5c, left) were shifted towards more negative potentials. The V_{rev} measured using the tail-current method is indicated by arrowhead. The V_{rev} was shifted in negative direction by lactate. The shift of ΔpH was calculated from the V_{rev} shift (ΔV_{rev}) using the linear relationship between V_{rev} and ΔpH (Fig. 1b). The ΔpH shift after NH_4Cl washout was ~0.8–0.9 U (Fig. 5b). The estimated ΔpH shift by lactate was increased dose-dependently (Fig. 5d). As the pH_o was decreased by 0.5 U, from 7.3 to 6.8, the pH_i drop could be evaluated by adding 0.5 U to the ΔpH shift. For example, the increase in ΔpH by 0.8 U at 150 mM means that the pH_i was reduced by approximately −1.3 U.

Progressive activation of the H^+ channel during prolonged lactic acidosis

As described above, an increase in ΔpH, the driving force for H^+ efflux, is a common mechanism to enhance the H^+ currents during cell acidosis induced by either washout of preloaded NH_4Cl or by application of Na-lactate. When the *I–V* curve obtained after the washout of NH_4Cl was moved positively to cancel the V_{rev} shift, the two *I–V* curves overlapped well (Fig. 5a, right). In this case, it is likely that the H^+ currents were enhanced mainly by the increase in the driving force for H^+. However, the two *I–V* curves, before and after stimulation with lactate, did not overlap (Fig. 5c right). The amplitudes of the currents at the same driving force were greater in the presence of lactate than those in the controls, suggesting that mechanisms other than increases in ΔpH may be involved in the lactate-induced activation of the H^+ channel. Prolonged exposure to lower concentrations (≤20 mM) of lactate revealed clearly that lactate activated the H^+ channel more strongly than expected from the ΔpH change itself: stable intracellular acidosis was attained within 5 min (Fig. 3a), but the H^+ currents continued to increase (Fig. 6a–c). Figure 6a shows a time course of progressive activation of the H^+ current with 10 mM lactate. The current reached the steady-state after 1 h. Although the increase in ΔpH by 10 mM lactate was only slight (Fig. 5d), the exposure for >1 h increased the current amplitude by approximately twofold (Fig. 6a–c). With 20 mM lactate, the current amplitude at >1 h was increased by approximately threefold (Fig. 6c), which was almost equal to the amount attained by 5-min exposure of 150 mM lactate.

To confirm the ΔpH-independent activation more clearly, whole-cell recordings were made in cells incubated with 20 mM lactate for >1 h. To stabilize ΔpH, pH_o and pH_i were set to be 7.3 and 5.5 with high concentrations (100–120 mM) of pH buffers. At a constant driving force, lactate enhanced the steady-state current amplitude by approximately twofold (Fig. 6d, left) and decreased τ_{act} to half (right). These results showed that properties of the H^+ channel per se were modulated so as to increase the H^+ current during long-lasting lactic acidosis.

PKC inhibitors prevent the late activation of the H^+ channel

Protein kinase C (PKC) is a strong activator for the H^+ channel [4, 20, 24]. Figure 7 summarizes the lactate (10 mM)-induced changes when the cells were preincubated with PKC inhibitors, staurosporine and chelerythrine. Both staurosporine (100 nM, >2 h) and chelerythrine (2 μM, >1 h) prevented the late increase in the amplitude of the steady-state current (a) and the lactate-induced decrease in τ_{act}. The

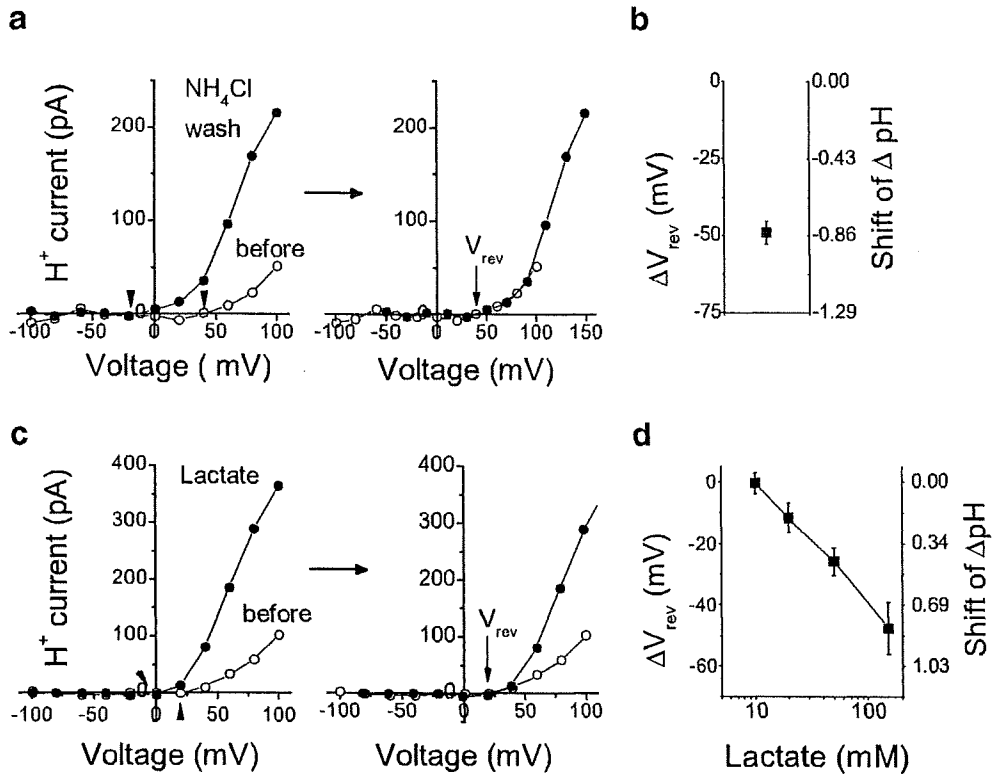

Fig. 5 Current–voltage (*I–V*) relationships and the reversal potentials (V_{rev}) of the H^+ channel during cell acidosis in the perforated-patch recordings. **a** *Left*, *I–V* plots for the steady-state current before (*open circles*) and after washout of pre-loaded NH_4Cl (*closed circles*). *Arrowheads* indicate V_{rev} estimated by the tail-current method (see "Materials and methods"). The two *I–V* curves were superimposed by moving the control curve to cancel the difference in the two V_{rev}s (*right*, *arrow*). **b** The shift of V_{rev} (ΔV_{rev}): −49±4 mV (n=4). The corresponding shift of ΔpH (0.84±0.06 pH unit, n=4) is indicated on the *right*. pH_o was maintained at 7.3 throughout the experiments. **c** *Left*, *I–V* relationships before (*open circles*) and after 5-min exposure to 50 mM Na-lactate (*closed circles*). *Right*, the *I–V* curve upon lactic acidosis was moved towards positive potentials to cancel the difference in the two V_{rev}s: **d** The shift of V_{rev} at 5-min exposure to lactate: −0.4±3.5 mV (n=6) for 10 mM, −12±5 mV (n=5) for 20 mM, −26±5 mV (n=6) for 50 mM, and −48±9 mV (n=6) for 150 mM corresponding to the shifts of ΔpH of 0.01±0.06, 0.20±0.08, 0.45±0.08, and 0.82±0.15 pH unit, respectively (on the right scale). pH_o was 7.3 in control and 6.8 in the presence of lactate. Data are means±SEM

inhibitory effects were more prominent at 1 h than those at 5 min The pretreatment with staurosporine or chelerythrine did not affect the H^+ current in the resting state.

Cell swellings and depolarization during prolonged lactic acidosis

Cell swelling is a potent activator for the H^+ channels in microglia [22]. In non-clamped cells, a 10-min exposure to 50 mM Na-lactate increased the cell diameter by ~10% (n=18–23). With 10–20 mM lactate, swelling developed more slowly: The diameter increased by 6.2±2.6% (n=10) with 10 mM and 8.9±2.7% (n=9) with 20 mM at 1 h. This level was maintained for several hours. Staurosporine did not prevent the cell swelling: 10 mM lactate increased the diameter by 6.7±4.1% (n=9) at 1 h even in cells treated with staurosporine (100 nM, 2 h).

The membrane potential recorded in the standard Ringer solution with K^+-containing pipette solution was −50± 10 mV (n=9) in control. There was no consistent change in the membrane potential after 5-min exposure to 20 mM lactate (−45±12 mV, n=8). However, the presence of 20 mM lactate for >1 h depolarized cells to about −10 mV (−12±5 mV, n=8) probably through metabolic disturbances. The depolarization might facilitate the channel openings.

Discussion

The H^+ channel is the most potent H^+-secreting mechanism among various transmembrane H^+ conduction pathways. Understanding the activation mechanisms is crucial in resolving the functional roles of the H^+ channel. The present study revealed that the H^+ channel was activated remarkably during lactic acidosis. The activation process was separated into two phases; an early enhancement due to increases in ΔpH and a later progressive potentiation through changes in properties of the channel per se.

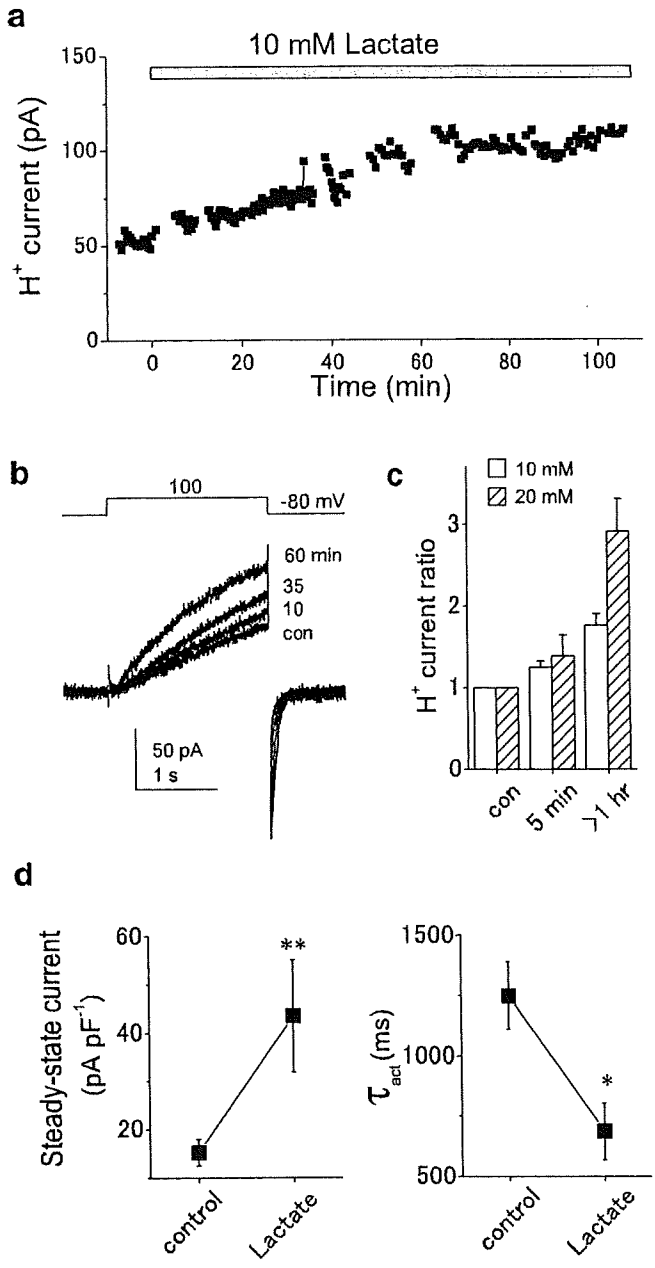

Fig. 6 Progressive activation of the H^+ channel during prolonged lactic acidosis. **a** A time course of gradual increases in H^+ currents in the presence of 10 mM lactate (pH 6.8). **b** H^+ currents (100 mV) recorded in a cell exposed to 10 mM lactate for 10, 35, and 60 min. **c** Relative H^+ current amplitude in cells after incubation with lactate for 5 min (n=4 for 10 mM, n=9 for 20 mM) and >1 h (n=4 for 10 mM, n=11 for 20 mM). The current amplitudes were measured at the end of 2- to 4-s-long depolarization pulses (80–100 mV) applied at −80 mV. **a**–**c** Obtained from perforated-patch recordings. **d** Whole-cell H^+ currents in control (n=5) and in cells incubated with 20 mM lactate (pH 6.8) for >1 h (n=13). pH_p/pH_o=5.5/7.3. Steady-state current-densities (*left*) and activation time constants (τ_{act}; *right*) were obtained from the responses evoked by depolarization pulses (40 mV) applied at −80 mV. The steady-state current and τ_{act} were 15.2±2.8 pA/pF, 1,250±140 ms for control, 43.5±11.6 pA/pF and 690±120 ms for the treated cells. Data are means±SEM. *p<0.05, **p<0.005

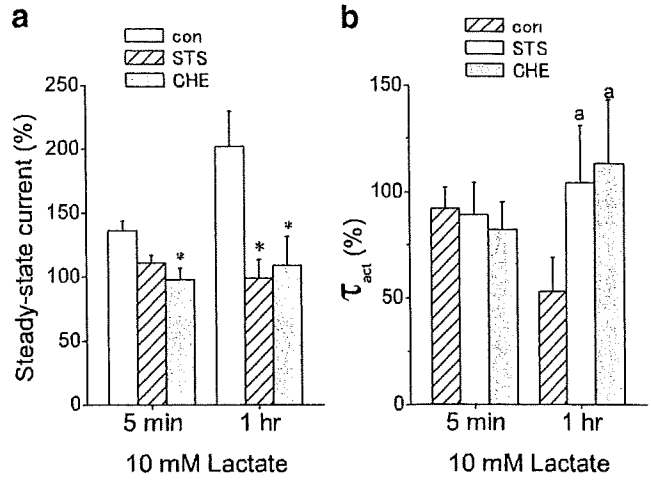

Fig. 7 Effects of PKC inhibitors on the lactate-induced activation of the H^+ current. Relative changes in the steady-state current amplitude (**a**) and τ_{act} (**b**) at 5-min and 1-h exposure to 10 mM lactate (pH 6.8). The data were obtained from the currents evoked by depolarization pulses to −100 mV. The holding potential was −80 mV. The data in cells incubated with 100 nM staurosporine for >2 h (n=3–6) or 2 μM chelerythrine for >1 h (n=4–7) were compared with those in untreated cells (n=4–8). *p<0.05. *a* indicates p=0.2

Cell acidosis introduced in the perforate-patch configuration The electrophysiological features of H^+ channels, well-characterized in the whole-cell condition, show that the activity of H^+ channels is regulated primarily by changes in ambient pH. Therefore, H^+ channels could function as pH sensors. However, the pH-monitoring actions of H^+ channels are distinct from those of acid-sensing channels like vanilloid receptors and ASIC in several features including voltage gating and absence of threshold pH. Moreover, the responsiveness to both pH_i and pH_o complicates the actions of H^+ channels. Purely extracellular acidification decreases the channel activity, but purely intracellular acidification enhances it. However, these conditions seldom occur. Rather, changes in pH_o and pH_i are inseparable and often change in parallel in tissue acidosis. In this study, we employed the perforated-patch recordings to examine the lactate-induced changes in ΔpH and the H^+ channel activity over a wide range of the concentration.

The whole-cell recordings are generally performed under a strict control of pH_i with very high concentrations (100–120 mM) of pH buffers. It has been questioned whether the H^+ channel could respond to pH disturbances as expected even with intrinsic intracellular buffers under the perforated-patch configuration. We checked the fidelity of the recording system from the responses by washout of preloaded NH_4Cl. This is a common experimental procedure to examine the effects of acid-load [13]: cell acidosis can be imposed without changes in pH_o. During the acute cell acidosis, activation of the channel started upon a drop

in intracellular pH and terminated at relief of the cell acidosis. The activation lasted as long as the cell acidosis was sustained. The channel behavior in the acutely induced cell acidosis was well explained by changes in the driving force for H^+: the H^+ current was potentiated by the increase of ΔpH which shifted the activation threshold to more negative voltages and increased the driving force for H^+.

An additional concern of the perforated-patch recordings was whether the constant pH of the pipette solution (pH_p 7.3) might affect introduction of cell acidosis by lactate. The present study showed that cell acidosis was maintained under the perforated-patch configuration as far as lactate was present. At closer inspection, however, the 10 mM lactate-induced shift of ΔpH estimated from the V_{rev} was smaller (~0.01 pH unit; Fig. 5d) than the value obtained by the measurement using BCECF in non-clamped cells (~0.1 pH unit; Fig. 3c). Thus, a small amount of cell acidification may be underestimated under the effect of the pH_p. In addition, the control pH_i calculated from the V_{rev} (17±4 mV, n=8) was ~7.6, higher than the resting pH_i estimated with BCECF in non-clamped cells (~7.3). Proton efflux during the tail current method might increase pH_i, as depletion of protonated buffers shifts the V_{rev} towards more positive voltages even in the whole-cell configuration under high concentrations of pH buffers [3]. Otherwise, absence of Cl^- in the electrophysiological recordings may be responsible for the difference at least partly [26]. In spite of these small variations, the lactate-induced shift of the ΔpH estimated by the two methods was not far different. It is thus likely that the pH responses in the presence of intrinsic intracellular buffers were almost preserved under the present recording conditions.

Lactic acidosis and H^+ channel activation During lactic acidosis, both pH_o and pH_i decreased simultaneously. According to the ΔpH dependence of the channel activity as described above, the activation may occur only when the intracellular acidification exceeds the extracellular acidification. The resultant increase in ΔpH and activation of the H^+ channel were both dose-dependent at 5-min exposure to lactate. The increase in driving force for H^+ seems to be responsible for this early activation.

The increased ΔpH was, however, not enough to explain all the responses produced by lactate. First, the temporal patterns of the changes in ΔpH and the channel activation were not consistent. The current amplitude continued to increase over >1 h, although the pH_i reached the steady-state within 5 min. Second, the increases in the H^+ currents were much greater than those predicted from the increase in the driving force. Therefore, additional mechanisms other than the increase in ΔpH appear to contribute to lactate-induced activation of the H^+ channel, particularly when the exposure to lactate is prolonged. Whole-cell recordings, which could clamp ΔpH with high pH buffers, confirmed the change in the electrophysiological properties of the H^+ channel. The concentration of lactate in the tissue would be less than 10–20 mM. The ΔpH-independent late activation may be more significant in pathological context.

Mechanisms for the late activation by lactate The mechanisms responsible for the ΔpH-independent activation have not yet been fully resolved, but there are several possibilities. Cell acidosis could affect various cellular processes, besides direct effects on ion channels or enzymes: It changes the fluidity of the plasma membrane [15], increases the level of strong free radicals [30], and modifies the cytoarchitecture [8]. Activation of PKC is a mechanism underlying cellular responses in tissue acidosis [16, 19, 27]. H^+ channels are activated by PKC [4, 20, 24]. Pretreatment with PKC inhibitors inhibited the late phase of the lactate-induced activation of the H^+ channel, suggesting that PKC might be involved in the activation process. In addition, cell swelling developed slowly in the presence of lower (10–20 mM) concentrations of lactate, which could also contribute to activation of the H^+ channel [22]. As the swelling was not prevented by staurosporine, activation of the H^+ channel might be mediated through different pathways during lactic acidosis.

Patho/physiological implications Tissue disorders are often accompanied by lactic acidosis, cell swelling, depolarization, and fever, all of which activate H^+ channels. Proton channels are rich in the plasma membrane of phagocytes which are involved in the defense mechanism. The activity of NADPH oxidase is pH-dependent and is inhibited by intracellular acidification [31]. Long exposure to lactate depolarized cells to about −10 mV: The H^+ channel would open if pH_i is lower than pH_o by at least ~0.15 U. Additionally, activation of PKC shifts the voltage dependence by about −40 mV [4, 20]. Potentiated H^+ efflux could contribute to a relief of the severe cell acidosis caused by the accumulation of metabolic acid and may hyperpolarize cells. H^+ channels are also essential for charge compensation during the respiratory burst which induces accumulation of intracellular H^+ and depolarization [5, 12, 23]. The activated H^+ channel may serve to maintain phagocytotic action of microglia during long-lasting metabolic acidosis.

Acknowledgements We would like to thank Dr. Charles Edwards for critically reading the manuscript, Y. Moriura and K. Hiraoka for technical assistance, and Y. Yoshioka and M. Okamoto for secretary assistance. This work was supported by a Grant-in-Aid for Scientific Research from The Ministry of Education, Science, and Culture, Japan.

References

1. Byerly L, Meech R, Moody W (1984) Rapidly activating hydrogen ion currents in perfused neurones of the snail, *Lymnaea stagnalis*. J Phyisol 351:199–216
2. Cohen RD, Woods HF (1983) Lactic acidosis revisited. Diabetes 32:181–191
3. DeCoursey TE (2002) Voltage-gated proton channels and other proton transfer pathways. Physiol Rev 83:475–579
4. DeCoursey TE, Cherny VV, Zhou W, Thomas LL (2000) Simultaneous activation of NADPH oxidase-related proton and electron currents in human neutrophils. Proc Natl Acad Sci USA 97:6885–6889
5. Demaurex N, Petheö GL (2005) Electron and proton transport by NADPH oxidases. Philos Trans R Soc B 360:2315–2325
6. Eder C, DeCoursey TE (2001) Voltage-gated proton channels in microglia. Prog Neurobiol 64:277–305
7. Eder C, Fischer HG, Hadding U, Heinemann U (1995) Properties of voltage-gated currents of microglia developed using macrophage colony-stimulating factor. Pflügers Arch 430:526–533
8. Faff L, Nolte C (2000) Extracellular acidification decreases the basal motility of cultured mouse microglia via the rearrangement of the actin cytoskeleton. Brain Res 853:22–31
9. Grinstein S, Furuya W (1988) Assessment of Na^+–H^+ exchange activity in phagosomal membranes of human neutrophils. Am J Physiol 254:C272–C285
10. Grinstein S, Goetz JD, Furuya W, Rothstein A, Gelfand EW (1984) Amiloride-sensitive Na^+–H^+ exchange in platelets and leukocytes: detection by electronic cell sizing. Am J Physiol 247:C293–C298
11. Gordienko DV, Tare M, Parveen S, Fenech CJ, Robinson C, Bolton TB (1996) Voltage-activated proton current in eosinophils from human blood. J Physiol (Lond) 496:299–316
12. Henderson LM, Chappell JB, Jones OT (1987) The superoxide-generating NADPH oxidase of human neutrophils is electrogenic and associated with an H^+ channel. Biochem J 246:325–329
13. Hoffmann EK, Simonsen LO (1989) Membrane mechanisms in volume and pH regulation. Physiol Rev 69:315–382
14. Immke DC, McCleskey EW (2001) Lactate enhances the acid-sensing Na^+ channel on ischemia-sensing neurons. Nat Neurosci 4:869–870
15. Kaila K, Ransom BR (1988) Concept of pH and its importance in neurobiology. In: Kaila K, Ransom BR (eds) pH and brain function. Wiley-Liss, New York, pp 3–10
16. Katsura K, Kurihara J, Siesjo BK, Wieloch T (1999) Acidosis enhances translocation of protein kinase C but not Ca^{2+}/calmodulin-dependent kinase II to cell membrane during complete cerebral ischemia. Brain Res 849:119–127
17. Kreisberg RA (1984) Pathogenesis and management of lactic acidosis. Annu Rev Med 35:181–193
18. Kuno M, Kawawaki J, Nakamura F (1997) A highly temperature-sensitive proton current in mouse bone marrow-derived mast cells. J Gen Physiol 109:731–740
19. Lubec B, Dell'Anna E, Fang-Kircher S, Marx M, Herrena-Marschitz M, Lubec G (1997) Decrease of brain kinase C, protein kinase A, and cyclin-dependent kinase correlating with pH precedes neuronal death in neonatal asphyxia. J Invest Med 45:274–294
20. Mori H, Sakai H, Morihata H, Kawawaki J, Amano H, Yamano T, Kuno M (2003) Regulatory mechanisms and physiological relevance of a voltage-gated H^+ channel in murine osteoclasts: phorbol myristate acetate induced cell acidosis and the channel activation. J Bone Miner Res 18:2069–2076
21. Morihata H, Kawawaki J, Sakai H, Sawada M, Tsutada T, Kuno M (2000) Temporal fluctuation of voltage-gated proton currents in rat spinal microglia via pH-dependent and -independent mechanisms. Neurosci Res 38:265–271
22. Morihata H, Nakamura F, Tsutada T, Kuno M (2000) Potentiation of a voltage-gated proton current in acidosis-induced swelling of rat microglia. J Neurosci 20:7220–7227
23. Murphy R, DeCoursey TE (2006) Charge compensation during the phagocyte respiratory burst. Biochim Biophys Acta 1757:996–1011
24. Nanda A, Grinstein S (1991) Protein kinase C activates a H^+ (equivalent) conductance in the plasma membrane of human neutrophils. Proc Natl Acad Sci USA 88:10816–10820
25. Rehncrona S (1985) Brain acidosis. Ann Emerg Med 14:770–776
26. Ringel F, Chang RC, Staub F, Baethmann A, Plesnila N (2000) Contribution of anion transporters to the acidosis-induced swelling and intracellular acidification of glial cells. J Neurochem 75:125–132
27. Rohra DK, Yamakuni T, Ito S, Saito S, Ohizumi Y (2004) Evidence for the involvement of protein kinase C in acidic pH-induced contraction in spontaneously hypertensive rat aorta. Pharmacology 71:10–16
28. Salimi K, Moser K, Zassler B, Reindl M, Embacher N, Schermer C, Weis C, Marksteiner J, Sawada M, Humpel C (2002) Glial cell line-derived neurotrophic factor enhances survival of GM-CSF dependent rat GMIR1-microglial cells. Neurosci Res 43:221–229
29. Siesjö BK (1988) Acidosis and ischemic brain damage. Neurochem Pathol 9:31–88
30. Siesjö BK, Bendek G, Koide T, Westerberg E, Wieloch T (1985) Influence of acidosis on lipid peroxidation in brain tissues in vitro. J Cereb Blood Flow Metab 5:253–258
31. Simchowitz L (1985) Intracellular pH modulates the generation of superoxide radicals by human neutrophils. J Clin Invest 76:1079–1089
32. Staub F, Beathmann A, Peters J, Weigt H, Kempski O (1990) Effects of lactoacidosis on glial cell volume and viability. J Cereb Blood Flow Metab 10:866–876
33. Thomas RC, Meech RW (1982) Hydrogen ion currents and intracellular pH in depolarized voltage-clamped snail neurons. Nature 299:826–828

THE JOURNAL OF BIOLOGICAL CHEMISTRY VOL. 283, NO. 12, pp. 7983–7993, March 21, 2008

Stimulus-dependent Regulation of the Phagocyte NADPH Oxidase by a VAV1, Rac1, and PAK1 Signaling Axis*[S]

Received for publication, October 4, 2007, and in revised form, December 17, 2007 Published, JBC Papers in Press, December 26, 2007, DOI 10.1074/jbc.M708281200

Kirstine Roepstorff[‡], Izabela Rasmussen[‡], Makoto Sawada[§], Cristophe Cudre-Maroux[¶], Patrick Salmon[¶], Gary Bokoch[‖], Bo van Deurs[‡], and Frederik Vilhardt[‡1]

From the [‡]Department of Cellular and Molecular Medicine, Faculty of Health Sciences, University of Copenhagen, 2200N Copenhagen, Denmark, the [¶]Department of Microbiology, Université de Genève, 1211 Genève, Switzerland, the [‖]Departments of Immunology and Cell Biology, Scripps Research Institute, La Jolla, California 92037, and the [§]Department of Brain Function, Research Institute of Environmental Medicine, Nagoya University, Nagoya 464-8601, Japan

The p21-activated kinase-1 (PAK1) is best known for its role in the regulation of cytoskeletal and transcriptional signaling pathways. We show here in the microglia cell line Ra2 that PAK1 regulates NADPH oxidase (NOX-2) activity in a stimulus-specific manner. Thus, conditional expression of PAK1 dominant-positive mutants enhanced, whereas dominant-negative mutants inhibited, NADPH oxidase-mediated superoxide generation following formyl-methionyl-leucyl-phenylalanine or phorbol 12-myristate 13-acetate stimulation. Both Rac1 and the GTP exchange factor VAV1 were required as upstream signaling proteins in the formyl-methionyl-leucyl-phenylalanine-induced activation of endogenous PAK1. In contrast, PAK1 mutants had no effect on superoxide generation downstream of FcγR signaling during phagocytosis of IgG-immune complexes. We further present evidence that the effect of PAK1 on the respiratory burst is mediated through phosphorylation of p47^{Phox}, and we show that expression of a p47^{Phox} (S303D/S304D/S320D) mutant, which mimics phosphorylation by PAK1, induced basal superoxide generation *in vivo*. In contrast PAK1 substrates LIMK-1 or RhoGDI are not likely to contribute to the PAK1 effect on NADPH oxidase activation. Collectively, our findings define a VAV1-Rac1-PAK1 signaling axis in mononuclear phagocytes regulating superoxide production in a stimulus-dependent manner.

The superoxide-generating phagocyte NADPH oxidase (NOX-2) consists of integral membrane subunits gp91^{Phox} and p22^{Phox} and cytosolic subunits p40^{Phox}, p47^{Phox}, p67^{Phox}, and the small GTPase Rac1 or Rac2. The gp91^{Phox} and p22^{Phox} proteins are permanently associated with each other in the membrane to form the catalytic flavocytochrome b_{558} core (cyt b_{558})[2] through which electrons from NADPH are transported to reduce molecular oxygen to superoxide on the external side. Only in activated phagocytes do the cytosolic factors translocate to the membrane to interact with cyt b_{558} and initiate superoxide production (1). *In vitro*, purified membranes containing cyt b_{558} demonstrate superoxide production when reconstituted with high concentrations of p67^{Phox} and prenylated, GTP-loaded Rac1 (2), as these two cytosolic factors regulate electron transfer from NADPH to cyt b_{558} (3). But *in vivo*, p47^{Phox} is essential for NADPH oxidase activity and serves to guide the p67^{Phox} subunit to the membrane. Upon cell activation, p47^{Phox} undergoes phosphorylation of multiple serine residues. This induces exposure of binding domains that can interact with p22^{Phox} (4) and phosphoinositide lipid products (5), thereby causing translocation of p47^{Phox}/p67^{Phox} to the membrane (6), presumably assisted by the actin cytoskeleton. Several kinases have been implicated in phosphorylation of p47^{Phox}, including Akt (7, 8), PKC isoforms (9), p38^{MAPK}, and ERK1/2 (10).

The small GTPase Rac1, a required catalytic subunit of the NADPH oxidase holoenzyme, translocates to the membrane with identical kinetics as p47^{Phox} and p67^{Phox} (11), but independently thereof (12–14). Several guanine nucleotide exchange factors (GEFs) for Rac1 have been implicated in NADPH oxidase activity in neutrophils or *in vitro*, including VAV1 (15) and P-Rex (16). An important effector molecule for Rac1 is the serine/threonine kinase p21-activated kinase (PAK1), which to a large extent mediates the effects of Rac1 and Cdc42 on the actin cytoskeleton (17). In the N-terminal part, PAK1 contains a small GTPase-binding site, the p21-binding domain (PBD; amino acids 67–150), partially overlapping with the so-called auto-inhibitory domain (AID; amino acids 83–149), which is thought to engage in intramolecular bonding

* This work was supported by Danish Research Council Grant 22-04-0336, grants from Scleroseforeningen and the Lundbeck Foundation (to F. V.), and National Institutes of Health Grant HL48008 (to G. B.). The costs of publication of this article were defrayed in part by the payment of page charges. This article must therefore be hereby marked "*advertisement*" in accordance with 18 U.S.C. Section 1734 solely to indicate this fact.

[S] The on-line version of this article (available at http://www.jbc.org) contains supplemental Figs. 1–4.

[1] To whom correspondence should be addressed: Dept. of Cellular and Molecular Medicine, Bldg. 18.4, The Panum Institute, Copenhagen University, Blegdamsvej 3, 2200N Copenhagen, Denmark. Tel.: 45-35327120; Fax: 45-35327285; E-mail: f.vilhardt@mai.ku.dk.

[2] The abbreviations used are: cyt b_{558}, flavocytochrome b_{558}; AA, arachidonic acid; BIM-1, bisindolylmaleimide-1; GEF, GTP exchange factor; LIMK, LIM kinase; NOS, NO synthetase; PAK, p21-activated kinase; PBD, p21-binding domain; fMLP, formyl-methionyl-leucyl-phenylalanine; PMA, phorbol 12-myristate 13-acetate; PKC, protein kinase C; mAb, monoclonal antibody; HA, hemagglutinin; PBS, phosphate-buffered saline; CHAPS, 3-[(3-cholamidopropyl)dimethylammonio]-1-propanesulfonic acid; GFP, green fluorescent protein; WT, wild type; PVDF, polyvinylidene difluoride; DPI, diphenyliodonium; HBSS, Hanks' balanced salt solution; FACS, fluorescence-activated cell sorter; MOPS, 4-morpholinepropanesulfonic acid; luminol E-CL, luminol-enhanced chemiluminescence; DHCF, 5,7-dichlorodihydrofluorescein.

with the C-terminal kinase domain of PAK1 thereby preventing activity. However, binding of activated (GTP-loaded) Rac1 or Cdc42 to the PBD relieves this allosteric inhibitory mechanism, freeing the kinase domain for activity (18).

It was recently shown that inhibition of PAK1 by the AID fragment exerts an inhibitory effect on the neutrophil respiratory burst (19). There are several putative mechanisms whereby PAK1 can affect NADPH oxidase activity, including RhoGDI phosphorylation (20) or regulation of actin dynamics involved in NADPH oxidase assembly. Furthermore, *in vitro* kinase assays have established that p47^{Phox} is a substrate of PAK1 (19, 21), but how PAK1 modulates the respiratory burst *in vivo* (19), and whether such an effect is exerted through phosphorylation of p47^{Phox}, remains unresolved.

In the following we have investigated the role of PAK1, and its immediate upstream regulators VAV1 and Rac1, in NADPH oxidase activation in murine microglia. Using lentivectors to achieve efficient conditional expression of wild type or dominant-negative or -positive mutants of PAK1, VAV1, and Rac1, we demonstrate that PAK1 function is required for NADPH oxidase-mediated superoxide production following fMLP (formyl-methionyl-leucyl-phenylalanine) stimulation and that this PAK1 activity depends on VAV1 and Rac1 as upstream signaling proteins. In contrast, we found no evidence for a role of PAK1 in IgG-immune complex-induced NADPH oxidase activation.

MATERIALS AND METHODS

The murine microglia cell line Ra2 (56) was maintained in minimum Eagle's medium with 10% fetal calf serum, 1 ng/ml granulocyte macrophage colony-stimulating factor (PeproTech, UK), and 5 μg/ml bovine insulin (22, 23). fMLP, phorbol 12-myristate 13-acetate, luminol, HRP-II, insulin, arachidonic acid, and diphenyliodonium (DPI) were purchased from Sigma. Bisindolylmaleimide-1 (BIM-1) and L-NMMA were from Calbiochem. Rabbit anti-PAK1 antibody, goat anti-Thr(P)-423 PAK1 antibody, and mouse anti-Myc mAb (clone 9E10) were from Santa Cruz Biotechnology; rabbit anti-PAK1 antibody was from Signal Transduction Laboratories; rabbit anti-PAK1 mAb was from Abcam; rabbit anti-PAK1, -2, and -3 were from Chemicon; mouse anti-HA tag mAb was from Sigma. Alexa 488-conjugated phalloidin, FcOxyburst, secondary Alexa 568- or 633-conjugated goat anti-mouse or goat anti-rabbit antibodies for immunofluorescence and FACS were from Molecular Probes.

Lentivector Construction—The cDNA of human origin for Myc-tagged PAK1 wild type, the dominant inhibitory mutants PAK1-K299A, PBD, PBD-H83L, and the dominant-positive PAK1-T423E and -H83L/H86L mutants (24), dominant-negative Myc-tagged VAV1-L213A (kindly provided by Dr. Amnon Altman, La Jolla Institute for Allergy and Immunology, La Jolla, CA), Rac1-V12 or Rac1-V12/Y40C (a generous gift of Dr. Mary Dinauer, Department of Microbiology and Immunology, Indiana University Medical School), wild type or mutant p47^{Phox}(S303D/S304D/S320D) of human origin (a kind gift of Dr. Hideki Sumimoto, Medical Institute of Bioregulation, Kyushu University, Japan), or HA-tagged dominant-negative Rac1-N17 (kindly provided by Dr. Emanuelle Caron, Division of Cell and Molecular Biology, Imperial College, London, UK) were PCR-amplified with primers to generate 5′ and 3′ restriction enzyme sites compatible with BamHI/SalI cloning into the lentiviral vector pLOX TW under the control of a tetracycline-responsive promotor (25). Human p47^{Phox}-GFP cDNA (a kind gift of Dr. Lance Terada, University of Texas, Southwestern Medical Center, Dallas) was PCR-amplified with primers for directional TOPO cloning into the lentiviral vector pLenti-6/V5/TOPO (Invitrogen). All constructs were verified by sequencing.

Lentivirus Production and Cell Transduction—Calcium phosphate transfection of HEK 293T producer cells and lentivector production has been described elsewhere (22). A Ra2 cell line referred to as 045 was established by transduction with lentivector pLOX TW rtTA (25), which expresses the tetracycline-inducible transactivator protein (rtTA). Following transduction of Ra2 045 with GFP-expressing vector pLOX TW GFP, more than 95% of the cells expressed high levels of GFP after overnight induction with 0.1–0.3 μg/ml doxycycline, conditions that were also used for induction of all rtTA-regulated transgenes in this study. By extrapolating results obtained from titering of pLOX TW GFP virus on Ra2 045 cells, we estimate that cells have received pLOX TW-PAK1, VAV1, Rac1, and p47^{Phox} lentivectors in a concentration of 20–40 multiplicities of infection, which resulted in high level expression of transgene in more than 90% of cells as estimated by immunofluorescence and FACS analysis with anti-Myc or anti-HA antibodies. In case of double transduction, PAK1-expressing Ra2 cells were superinfected with VAV1-L213A, Rac1-N17, or p47^{Phox}-GFP-expressing lentivectors as specified.

Cell Lysis, Immunoprecipitation, and Two-dimensional Gel Electrophoresis—To analyze phosphorylation of endogenous murine PAK1, Ra2 microglia in suspension in HBSS were stimulated with 4 μM fMLP at 37 °C, and aliquots withdrawn at intervals were plunged into ice-cold PBS to stop the reaction. Following centrifugation, and lysis of pellet in RIPA buffer (150 mM NaCl, 1 mM EDTA, 0.1% SDS, 1% deoxycholate, 1% Nonidet P-40, 50 mM MOPS, pH 8) with phosphatase and protease inhibitors (Sigma), immunoprecipitation with anti-PAK1 antibodies was carried out as described below. To analyze the effect of dominant-negative VAV1 and Rac1 on PAK1 activation, Ra2 microglia overexpressing PAK1 wild type alone, or in combination with either dominant-negative VAV1-L213A or Rac1-N17, were suspended in HBSS and stimulated with 2.5–5 μM fMLP at 37 °C for 2 min. Stimulation was stopped by addition of a large volume of ice-cold PBS. Following centrifugation and lysis of cell pellet in RIPA buffer, the precleared lysate was incubated with protein A-conjugated Sepharose beads and rabbit anti-PAK1 antibodies (4 μg/ml) overnight at 4 °C. Beads were washed in RIPA buffer, resuspended in Laemmli sample buffer for subsequent electrophoresis, and Western blotted with rabbit or goat antibody specifically recognizing PAK1 phosphorylated at Thr-423 or mouse antibody recognizing the Myc tag of PAK1 wild type. For two-dimensional gel electrophoresis, Ra2 microglia were harvested and washed in PBS, pelleted, and lysed in 5 M urea, 2 M thiourea, 2% CHAPS, 2% SB3-10, and 40 mM Trizma (Tris base), pH 10.1. After lysis, reduction with 4 mM tributylphosphine and alkylation of the samples with 15

mM iodoacetamide, aliquots were adjusted for protein concentration (Bio-Rad) and appropriate ampholytes (Bio-Rad) added. Then, 11-cm, pH 3–10, IPG strips (Bio-Rad) or pH 6–11 IPG strips (Sigma) were equilibrated overnight with 150 μl of lysate containing 300 μg of protein. Alternatively, for p47^{Phox}-GFP immunoprecipitates, 11-cm, pH 5–8 or pH 4–7, IPG strips (Bio-Rad) were used. The next day isoelectric focusing (15,000–20,000 V-h for neutral pH strips and 70,000–80,000 V-h for pH 6–11 strips) and second dimension electrophoresis on 12.5% SDS-polyacrylamide gels was performed. Protein was subsequently semidry-transferred to PVDF membranes and Western-blotted with anti-RhoGDI mAb (Transduction Laboratories) or polyclonal rabbit anti-p47^{Phox} antibodies (from Santa Cruz Biotechnology; and kindly provided by Dr. Bill Nauseef, University of Iowa, Iowa City, IA, and Dr. Frans Wientjes, Dept. of Medicine, University College London, UK). Signal was developed with appropriate secondary horseradish peroxidase-conjugated antibodies using ECL (Amersham Biosciences).

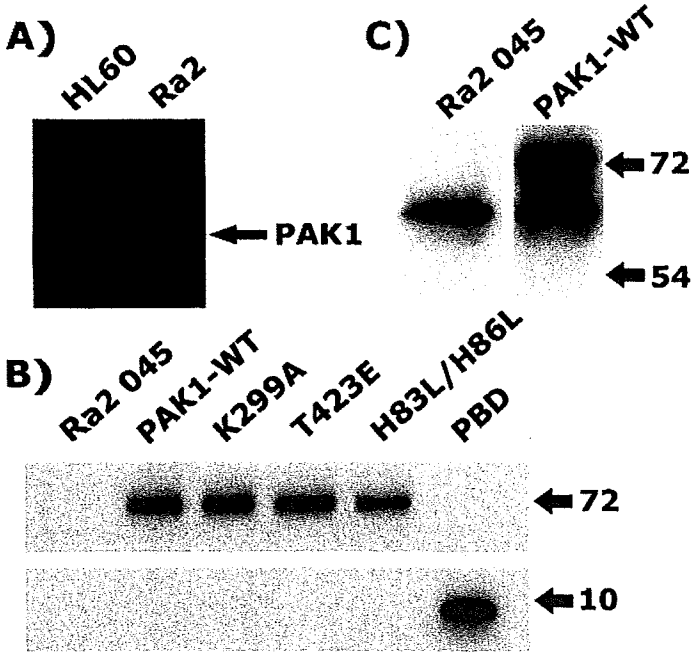

FIGURE 1. **Ra2 microglia conditionally express Myc-tagged PAK1 wild type and mutant protein following lentivirus gene transfer.** *A*, Triton X-100 detergent cell extracts of human promyelocytic HL60 cells and murine microglia cell line Ra2 were Western-blotted with an antibody recognizing PAK1, -2, and -3. In HL60 cells PAK1, and either PAK2 or PAK3, are detected but Ra2 microglia express only PAK1 (see *C*). *B*, PAK1 wild type and mutant protein expression was induced overnight in Ra2 microglia transduced with doxycycline-responsive lentivectors, and transgene levels were determined by Western blotting with anti-Myc antibodies. Control cells Ra2 045 express only the doxycycline-binding rtTA-transactivator protein. *C*, Triton X-100 extracts of Ra2 045 control cells and Ra2 PAK WT cells were Western-blotted with a polyclonal rabbit anti-PAK1 antibody to indicate the degree of overexpression of PAK-WT (*upper band* in *PAK WT lane*) in relation to endogenous PAK1 (*lower band*). The Western blots are representative of two (*A*) or three independent experiments.

Measurement of Superoxide Production—Luminol-enhanced chemiluminescence was used to measure fMLP- or PMA-induced superoxide release as described previously (26) with the exception that luminescent signal was measured in a thermostated Synergy HT microplate reader equipped with an injection module. Ra2 microglia in HBSS buffer on ice were warmed 1–2 min in a 37 °C water bath before dispensing into microtiter plates (Wallac black isoplates) at 100,000 cells/well. Subsequently, superoxide production of cells in suspension (plates were intermittently shaken to prevent cell lodging) was measured every 5–9 s at 37 °C before and after stimulation with 4 μM fMLP or 100 ng/ml PMA (final concentrations) delivered through the injector module. Alternatively, Ra2 cells were preincubated with or without 200 nM BIM-1 for 5 min before injection of arachidonic acid at a final concentration of 10 μM and measurement as above. To measure superoxide emitted during FcγR-mediated phagocytosis, we used 5,7-DHCF-conjugated bovine serum albumin-IgG immune complexes (FcOxyburst, Molecular Probes), which form aggregates sufficiently large to be phagocytosed. One million Ra2 cells were incubated with FcOxyburst at a concentration of 50 μg/ml in a volume of 300 μl of HBSS on ice for 1 h, briefly centrifuged at low speed, resuspended, and then kept on ice in the dark until FACS analysis. Reaction was started by adding an excess of 37 °C HBSS containing a low concentration of goat anti-rabbit Alexa 633 antibodies to identify and gate cells with bound IgG aggregates. The cells were placed in a 37 °C thermostated chamber of a FACS Aria (BD Biosciences) equipped with laser lines of 488 and 633 nm to excite 5,7-DHCF and Alexa 633, respectively, and emission filters for fluorescein isothiocyanate and allophycocyanin detection, respectively. Cells with bound IgG aggregates (~50% of total population, little variation between cell lines) were gated, and fluorescence intensity of 5,7-DHCF was sampled for 3000–5000 cells every 3rd min for up to 9 min. Mean fluorescence intensity of goat -anti-rabbit Alexa 633 after 30–60 s of mixing with antibodies was taken as measure of IgG-aggregate binding capacity of the cells, and 5,7-DHCF fluorescence was normalized to this value. Under the conditions used, 10 μM DPI or 1 mM L-NMMA inhibited 5,7-DHCF fluorescence emission by 90 and 52%, respectively.

Immunofluorescence—Ra2 cells were fixed in 2% paraformaldehyde in phosphate buffer, pH 7.2, permeabilized with 0.2%

TABLE 1
Mutants used and their phenotypes

Protein name	Phenotype	Rac1 binding	PAK1 binding	Activity
PAK1-WT	Wild type protein	Yes		Regulated kinase activity
PAK1-T423E	Dominant-positive	Yes		Constitutive kinase activity, high
PAK1-H83L/H86L	Dominant-positive	No		Constitutive kinase activity, moderate
PAK1-K299A	Dominant-negative	Yes		Kinase-dead
PBD (amino acids 83–149)	Dominant-negative	Yes		No kinase domain
PBD-H83L	Dominant-negative	No		No kinase domain
Rac1-N17	Dominant-negative		No	GEF binding (negative titration)
Rac1-V12	Dominant-positive		Yes	GTP-bound, no hydrolysis
Rac1-V12/Y40C	Dominant-positive		No	GTP-bound, no hydrolysis
VAV1-L213A	Dominant-negative			No GEF activity

saponin, and immunocytochemistry essentially performed as described (27) with mouse anti-Myc mAb to detect PAK1, mouse anti-HA mAb to detect Rac1-N17, and Alexa 488-conjugated phalloidin to visualize fibrillary actin. Images were acquired with a Zeiss LSM510 confocal laser scanning microscope with a C-Apochromat ×63, 1.2 oil immersion objective, using the 488 nm argon and 543 nm helium-neon laser lines for excitation of Alexa 488 and 568, respectively. Confocal sections (1.0–1.5 μm) were collected and saved as 512 × 512-pixel images at 8-bit resolution before import into Adobe Photoshop for compilation.

RESULTS

Conditional Expression of Wild Type and Mutant PAK1 Protein in Murine Microglia Cell Line Ra2—The established Ra2 murine microglia cell line (23) has been extensively used in our laboratory as it has a morphological phenotype resembling that of primary microglia and has retained capacity for stimulated cytokine (23) and superoxide production (22). We investigated PAK isoform expression in these cells using PAK1-specific antibodies and a pan-PAK antibody recognizing a domain highly conserved in PAK1, -2, and -3 isoforms. Human HL60 cells were included for comparison. As seen in Fig. 1*A*, Ra2 cells expressed only PAK1 protein, whereas HL60 cells expressed PAK1 and either PAK2 or -3. For further analysis, Ra2 microglia were transduced with lentivector expressing the tetracycline-transactivating response protein (rtTA) and the resulting subline named Ra2 045. These cells were subsequently superinfected with lentiviral vectors expressing human wild type or mutant PAK1 protein, including PAK1-K299A, PBD (p21-binding domain), PAK1-T423E, and PAK1-H83L/H86L (see Table 1 for an overview of mutants used in this study) under the control of the rtTA/doxycycline-responsive promotor (25). N-terminal Myc tagging allowed for easy detection of transgene expression by Western blotting and immunofluorescence (see Fig. 1, *B* and *C*, and Fig. 2).

Morphological Effect of PAK1 Wild Type and Mutant Protein in Microglia—PAK1 is well known to regulate cytoskeletal dynamics in mesenchymal cell types (28–30). To further verify the effect of expressed PAK1 transgenes, we therefore examined F-actin distribution by phalloidin staining in Ra2 cells expressing the various PAK1 mutants. Neither PAK1 wild type nor the K299A or PBD-H83L dominant-negative mutant proteins had any major effect on overall structure of the actin cytoskeleton (Fig. 2) but could be seen to colocalize with actin in cortical structures. In contrast, PAK1-T423E had a tendency to induce plasma membrane "blebbing," whereas the other active mutant PAK1-H83L/H86L greatly increased the extension of broad lamellipodia. The blebbing induced by PAK1-T423E expression was only present in a subpopulation of cells and did not result in increased cell death. Interestingly, this phenotype is indistinguishable from that of overexpression of the PAK1 substrate LIMK-1 alone (data not shown) and indicates that PAK1-T423E and -H83L/H86L differentially activate PAK1 targets that control cytoskeleton dynamics. For comparison, expression of dominant-negative Rac1-N17 induced collapse of the actin cytoskeleton into a cortical patch causing

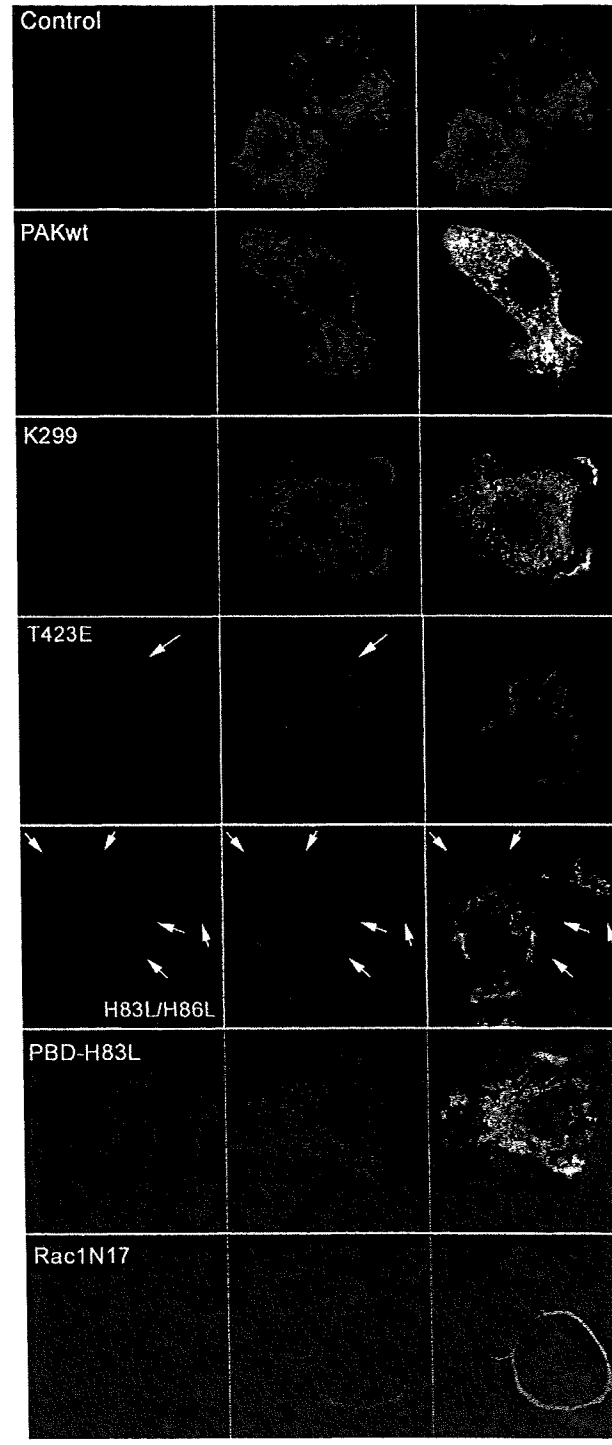

FIGURE 2. **Effect of PAK1 wild type and mutant protein on the actin cytoskeleton in Ra2 microglia.** Transduced PAK1 protein in the different Ra2 cell populations was visualized by immunofluorescence using α-Myc antibodies (*red*) to localize transgene PAK and Alexa 488-conjugated phalloidin to stain filamentous actin (*green*). Neither PAK1 wild type, K299A, nor PBD-H83L caused major alterations of the fibrillary actin cytoskeleton. On the other hand dominant-positive PAK1-T423E induced blebbing of the plasma membrane (*arrows*) in a high proportion of cells, whereas PAK1-H83L/H86L promoted extension of broad lamellipodia (*arrows*). For comparison, expression of dominant-negative Rac1-N17, visualized with α-HA tag antibodies (*red*), caused complete cell rounding with loss of ruffles, filopodia, and lamellipodia. *Bars* in all panels are 10 μm. The shown images are representative of at least three independent experiments.

rounding of cells and inhibition of lamellipodia, filopodia, and membrane ruffle formation. Collectively the data indicate that PAK1 mutants were functional in Ra2 cells and resulted in specific cytoskeletal phenotypes. As there is a correlation between actin dynamics and NADPH oxidase function (31–33), all subsequent analysis on the function of NADPH oxidase in the Ra2 cells was performed with the cells in suspension to minimize the interference from these different PAK1-mediated morphological phenotypes.

PAK1 Mutants Alter fMLP-mediated NADPH Oxidase Activation—We have shown previously that Ra2 microglia express all subunits of the phagocyte NADPH oxidase and produce superoxide in response to common stimulators of the respiratory burst (22), including fMLP, which in neutrophils is known to induce PAK1 activation (21). We therefore examined the fMLP-induced respiratory burst by luminol-enhanced chemiluminescence (luminol E-CL) in Ra2 cells transduced with wild type or mutant PAK1, including the auto-inhibitory PBD fragment of PAK1. This region of PAK1 (amino acids 67–150) contains both the auto-inhibitory domain of PAK1 (also called AID), and binding sites for small GTPases Rac1 and Cdc42. As shown in Fig. 3, *A* and *B*, expression of PAK1 wild type and the K299A mutant did not have a major effect on the respiratory burst, although PAK1-K299A consistently delayed the response. In contrast, expression of the PBD fragment inhibited superoxide production almost completely, and expression of PAK1-T423E and -H83L/H86L caused more than a 2-fold increase in superoxide release. To exclude that PBD, which binds both Rac1 and PAK1, was exerting its inhibitory effect by sequestering GTP-loaded Rac1, we also analyzed the effect of the PBD-H83L mutant that does not interact with Rac1 but retains binding and inhibitory activity toward PAK1. As seen in Fig. 3*C*, expression of PBD-H83L caused a dose-dependent decrease in superoxide generation, showing that the negative effect of PBD is mediated by repression of PAK1 function. In this (Fig. 3*C*) and most other figures with superoxide measurements, we have used luminol E-CL as a dynamic and highly sensitive probe for superoxide production. Depending on the presence of intracellular peroxidases and NO synthetase, luminol may also react with hydrogen peroxide, hydroxyl radicals, and peroxynitrite, albeit with different quantum yields. We have previously observed that addition of L-NMMA, an inhibitor of NO synthetase, reduces the luminol E-CL signal by 20–30% (22). As the signal is blocked 90–95% by superoxide dismutase, DPI, or expression of Rac1-N17, superoxide is clearly critical for luminol E-CL in Ra2 cells, and we assume the L-NMMA sensitive fraction of the E-CL signal represents formation of peroxynitrite, the reaction product of superoxide, and NO. As shown in supplemental Fig. 1, the ratio of the E-CL signal produced by L-NMMA-treated over non-treated cells did not significantly differ between control cells and the different PAK1 cell lines. This indicates that the luminol E-CL assay in Ra2 cells measures preferentially superoxide, and that differences in luminol E-CL signal observed reflect a differential effect of PAK1 mutants on NADPH oxidase activity, and only to a minor extent NO production.

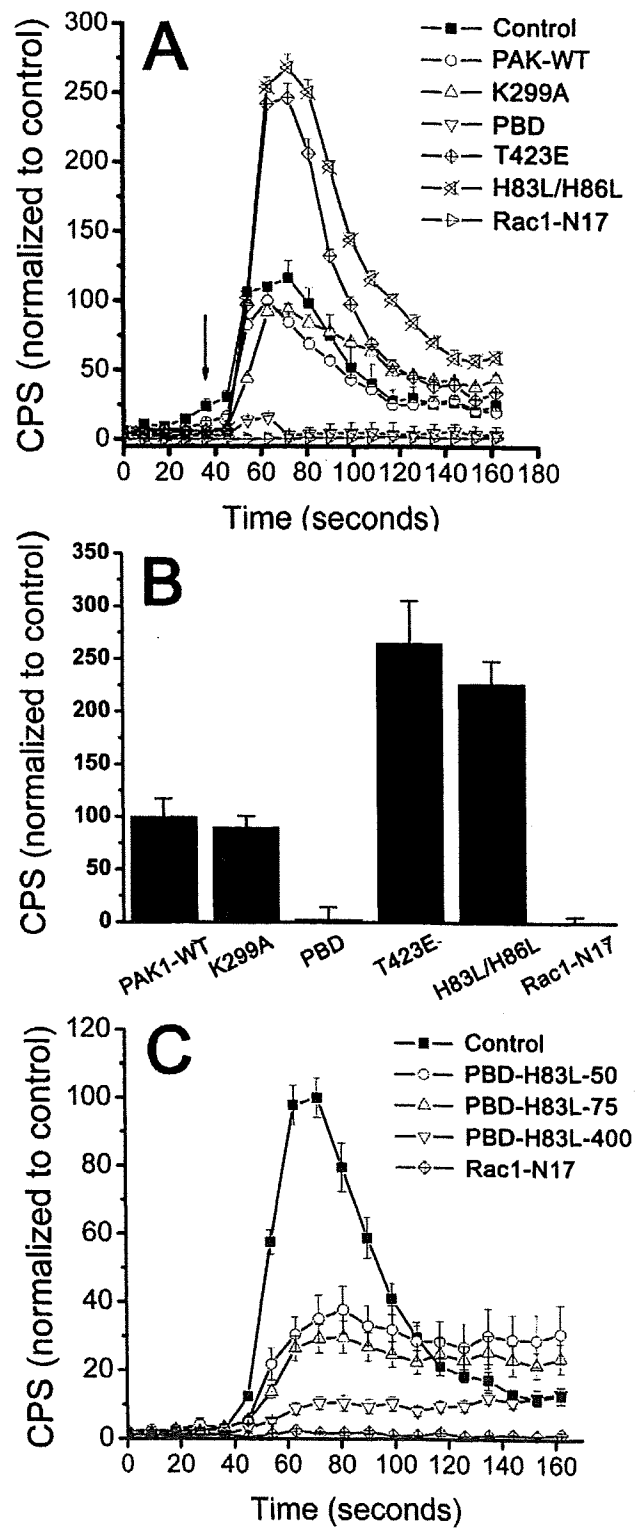

FIGURE 3. **PAK1 regulates superoxide production following fMLP stimulation.** *A*, fMLP-induced superoxide release in Ra2 cells expressing PAK1 wild type or mutant protein was measured by luminol E-CL. The *ordinate* shows chemiluminescent counts/s normalized to control cells, which were chosen as PAK1 WT-expressing cells. *Arrow* marks time point of fMLP injection. Results are presented as mean ± S.E. of an individual experiment performed in quadruplicate wells. *B*, mean ± S.E. of peak response of four separate experiments performed as above. *C*, Ra2 cells transduced with increasing concentrations of PBD-H83L lentivector (50, 75, and 400 μl) were inhibited in fMLP-stimulated superoxide production in a dose-dependent manner. The graph shows mean ± S.E. from a single experiment performed in triplicate and is representative of a total of two independent experiments.

Rac1 GTP Exchange Factor VAV1 Is Required for fMLP-induced PAK1 Activation and NADPH Oxidase Activation in Ra2 Microglia Cells—Several GEFs have been linked to NADPH oxidase activation in neutrophils, including VAV1 (15). To investigate whether the same GEF would be responsible for activation of Rac1 in its role as a catalytic subunit of NADPH oxidase, as well as an activator of PAK1, Ra2 cell lines conditionally expressing dominant-negative Rac1-N17 or dominant-negative VAV1-L213A (Fig. 4*A*) were analyzed for superoxide production and PAK activation following fMLP challenge. As seen in Fig. 4*B*, VAV1-L213A exerted a dose-dependent negative effect on the magnitude of superoxide release, attaining almost complete inhibition at the highest expression levels. This indicates that VAV1 in microglia is an important GEF involved in NADPH oxidase activation following stimulation with fMLP.

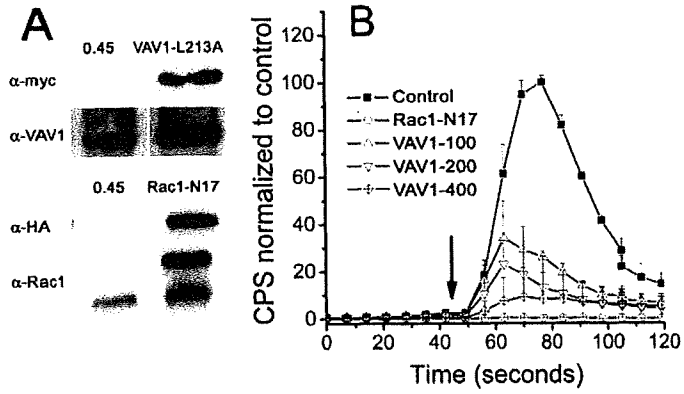

FIGURE 4. **VAV1 is required for fMLP-stimulated NADPH oxidase activity in Ra2 microglia.** *A*, Triton X-100 extracts of Ra2 cells expressing VAV1-L213A or Rac1-N17 were Western-blotted with antibodies to Myc or HA tags and with antibodies against VAV1 or Rac1, respectively. *B*, fMLP-induced superoxide production was measured by luminol E-CL in Ra2 045 control cells or cells transduced with increasing concentrations of lentivector conditionally expressing dominant-negative VAV1-L213A. *Arrow* points to time point of fMLP injection. Note the titer-dependent inhibition of superoxide production. For comparison, expression of dominant-negative Rac1-N17 entirely abrogated superoxide production. Mean ± S.E. of three independent experiments each performed in triplicate is shown.

When Ra2 microglia were stimulated with fMLP, endogenous PAK1 was transiently activated (Fig. 5, *A* and *B*) as determined by antibodies specific to phosphothreonine 423, which is autophosphorylated upon PAK1 activation (18). To decide whether the fMLP-induced PAK1 activation observed was a result of VAV1 and Rac1 signaling, we created cell lines coexpressing PAK1 wild type protein with either Rac1-N17 or VAV1-L213A (all conditionally expressed). As seen in Fig. 5, *C* and *D*, stimulation with fMLP induced auto-phosphorylation of PAK1 in cells expressing PAK1 wild type alone. However, coexpression of either dominant-negative VAV1 or Rac1 abrogated the fMLP-induced PAK1 auto-phosphorylation, indicating that VAV1 and Rac1 are necessary also for fMLP-induced PAK1 activation.

Effect of PAK1 Wild Type or Mutants on PMA-stimulated NADPH Oxidase Activation—Phorbol esters cause phosphorylation of p47^{Phox} and evoke a solid respiratory burst in phagocytes. When Ra2 microglia in suspension were stimulated with PMA (Fig. 6), the positive effect of the PAK1-H83L/H86L mutant on the magnitude of superoxide production was again evident, and additionally the lag time from stimulus to commencement of superoxide production was decreased. Curiously, the dominant-negative K299A mutant, which did not significantly depress the fMLP-mediated superoxide release, caused a 50% decrease in the case of PMA stimulation. Furthermore, the strong enhancing effect of PAK1-T423E seen after fMLP stimulation was absent, and PBD-H83L, which exerted a strong inhibition of the fMLP response, caused only a slight inhibition of the PMA-induced response. As before, Rac1-N17 entirely blocked superoxide generation. It can be added that in a FACS-based assay for superoxide production, we found no effect of PAK1 mutant expression following stimulation of NADPH oxidase by IgG-immune complexes, which bind and signal through FcγRs (supplemental Fig. 2).

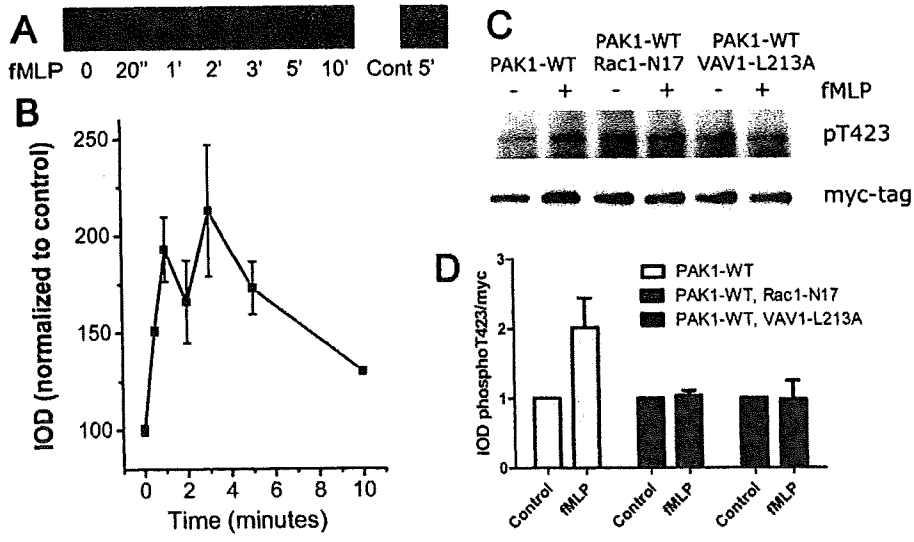

FIGURE 5. **fMLP activation of PAK1 depends on VAV1 and Rac1 signaling.** *A*, untransduced Ra2 cells were stimulated with 2.5 μM fMLP in suspension, and at intervals cell aliquots were withdrawn for Triton X-100 extraction, immunoprecipitation of endogenous PAK1, electrophoresis, and Western blotting with antibodies detecting PAK1-T423 auto-phosphorylation. One Western blot representative of three is shown. *B*, mean ± S.E. band intensity of three individual experiments performed as in *A* is shown. *C*, Ra2 cell lines expressing PAK1 wild type protein alone, or together with VAV-L213A or Rac1-N17, were established and stimulated with fMLP. Subsequently, the level of activated PAK1 in PAK1 immunoprecipitates was determined by Western blotting with phospho-PAK1-Thr-423 specific antibodies. Total PAK1 was also detected with anti-Myc antibodies as load control. The Western blot shown is representative of three individual experiments. *D*, densitometric analysis of three experiments performed as above. Mean ± S.E. of phospho-PAK1/total-PAK1 ratios is shown.

To further substantiate a role for PAK1 in NADPH oxidase activation, we created Ra2 cell lines conditionally expressing Rac1-V12 or Rac1-V12/Y40C. Both of these Rac1 mutants are constitutively active, but the Rac1-V12/Y40C mutant is incapable of binding and thereby activating endogenous PAK1. As seen in

Effect of Dominant-positive Rac1-V12 and Rac1-V12/Y40C Mutants on NADPH Oxidase Activation—

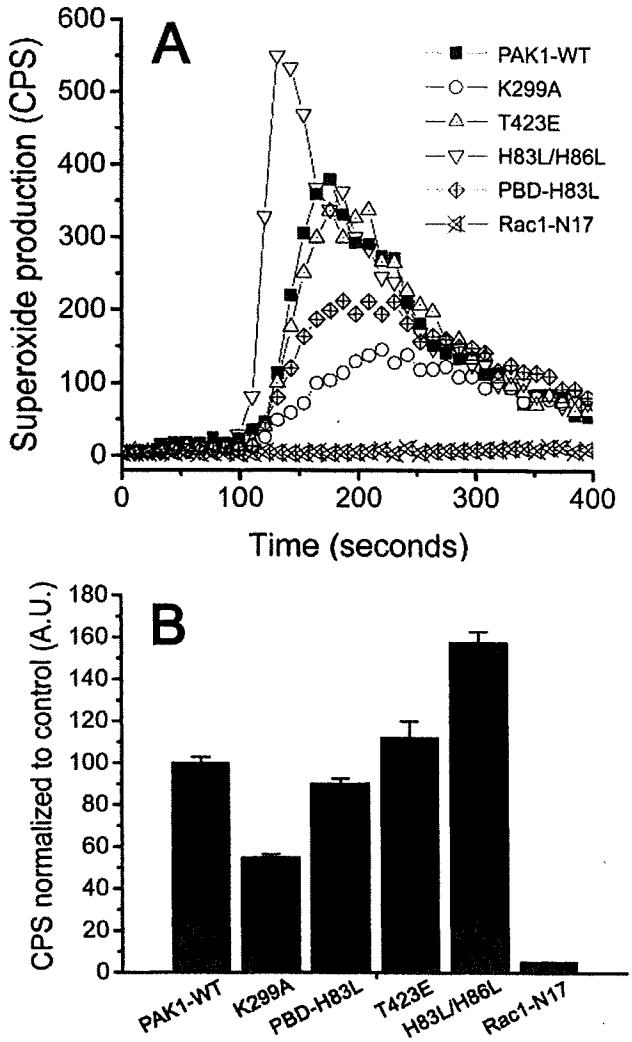

FIGURE 6. **PAK1 modulates PMA-stimulated superoxide production in microglia.** *A*, superoxide production of PMA-stimulated Ra2 microglia expressing wild type or mutant PAK1 protein or Rac1-N17 was measured by luminol E-CL. A single representative replicate from one of four independent experiments is shown. *B*, mean ± S.E. of superoxide production peak response as measured above. Results are presented as chemiluminescent signal normalized to control. Data were derived from four independent experiments performed in triplicate or quadruplicate.

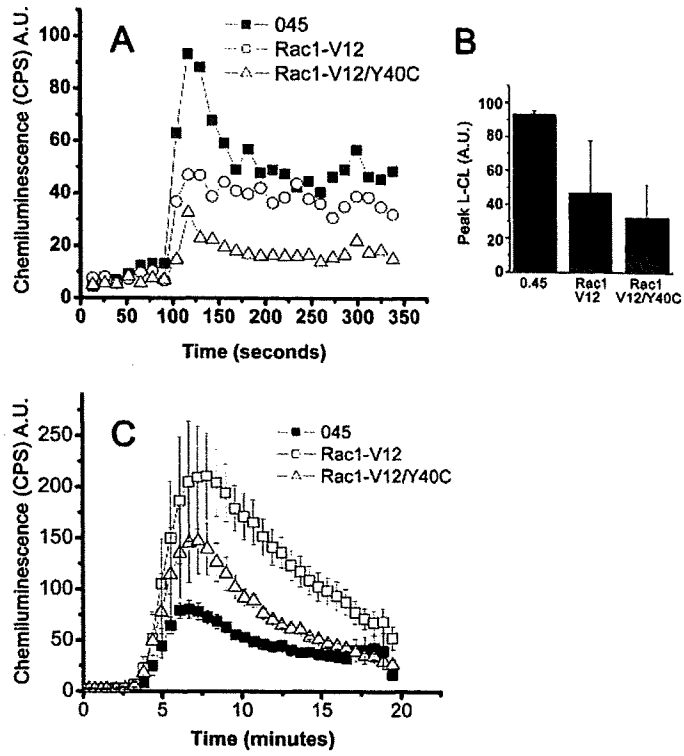

FIGURE 7. **Constitutively active mutants of Rac1 that differentially activate PAK1 have different effects on PMA-stimulated NADPH oxidase activation.** fMLP- (*A* and *B*) or PMA (*C*)-stimulated superoxide production of Ra2 045 control, Rac1-V12, or Rac1-V12/Y40C-expressing cells was measured by luminol E-CL. Traces from a single well are shown in *A*, the *traces* in *C* and the *bar graph B* represent in arbitrary units the mean ± S.E. of superoxide generation of three independent experiments, each performed as duplicate wells in triplicate runs.

Fig. 7, *A* and *B*, both Rac1 mutants inhibited the fMLP-induced respiratory burst with ~50%. When PMA was used as stimulus, however, both of the mutants increased the superoxide release, Rac1-V12 being the most effective (Fig. 7*C*).

Expression of Dominant-positive PAK1 Mutants Increase Phosphorylation of p47^{Phox} but Not RhoGDI—A direct way for PAK1 to influence the respiratory burst is by phosphorylation and activation of p47^{Phox}, which is a substrate of PAK1 *in vitro* (21).

We therefore examined phosphorylation of endogenous p47^{Phox} in Ra2 cells expressing PAK protein by two-dimensional gel electrophoresis and Western blotting. Cell lysates were subjected to isoelectric focusing using pH 3–10 or pH 6–11 strips as described under "Materials and Methods," and subsequently electrophoresed by SDS-PAGE and transferred to PVDF membranes for Western blotting with polyclonal anti-p47^{Phox} antibodies. As seen in Fig. 8*A*, only PAK-H8386L expressing cells showed consistent evidence of phosphorylation of p47^{Phox}, as judged by the appearance of two to three anodic (more acidic) species of p47^{Phox} not present in Ra2 045 control cells or PAK1-K299A or PAK1 WT-expressing cells. These data are supported by initial studies of p47^{Phox} phosphorylation in transfected HEK293 cells and Ra2 cells coexpressing the different PAK proteins with a GFP-p47^{Phox} fusion protein (supplemental Figs. 3 and 4). In contrast, by two-dimensional gel electrophoresis we found no indication that any of the PAK1 mutants appreciably affected phosphorylation of endogenous RhoGDI (Fig. 8*B*), which constitutes another PAK1 target with potential to influence NADPH oxidase activation via regulation of Rac1 nucleotide exchange.

PAK1-H83L/H86L Expression Synergizes with Arachidonic Acid in NADPH Oxidase Activation—It is largely accepted that phosphorylation causes p47^{Phox} to unfold from its closed conformation and expose binding sites for p22^{Phox} and phosphoinositides in the membrane (5, 6). It has been proposed that p47^{Phox} unfolds in two successive steps (interruption of C- and N-terminal interactions, respectively, with tandem SH3 domains in the middle of p47^{Phox} responsible for p22^{Phox} binding), based on the observation that low concentrations of arachidonic acid (AA), not sufficient for full p47^{Phox} unfolding, synergize with phosphorylation (by PKC) in NADPH oxidase activation (34). We therefore tested whether AA at low concentrations would synergize with dominant-positive PAK1 mutants in the induction of NADPH oxidase activity. Because